Variable Neural Adaptive Robust Control: A Switched System Approach

Jianming Lian, *Member, IEEE*, Jianghai Hu, *Member, IEEE*, and Stanislaw H. Żak, *Member, IEEE*

***Abstract*— Variable neural adaptive robust control strategies are proposed for the output tracking control of a class of multi-input multioutput uncertain systems. The controllers incorporate a novel variable-structure radial basis function (RBF) network as the self-organizing approximator for unknown system dynamics. It can determine the network structure online dynamically by adding or removing RBFs according to the tracking performance. The structure variation is systematically considered in the stability analysis of the closed-loop system using a switched system approach with the piecewise quadratic Lyapunov function. The performance of the proposed variable neural adaptive robust controllers is illustrated with simulations.**

***Index Terms*— Adaptive robust control, piecewise quadratic Lyapunov function, self-organizing approximator, uncertain system, variable-structure neural network.**

I. Introduction

MATHEMATICAL models used for controller design often contain uncertainties resulting from unknown system dynamics or disturbances. Several adaptive control strategies, such as adaptive feedback linearization [1], adaptive backstepping [2], nonlinear damping and swapping [3], and switching adaptive control [4], have been proposed for uncertain systems. In particular, a number of adaptive controllers were developed for a class of feedback linearizable nonlinear systems, including both single-input single-output (SISO) systems [5]–[8] and multiinput multioutput (MIMO) systems [9]–[12]. Most of the existing adaptive controllers [5]–[7], [9], [10], [12], [13] are state feedback controllers. However, it is often the case that only the system outputs are available. To overcome this problem, state observers have been utilized in the synthesis of output feedback based controllers. For example, high-gain observers have been employed in [8] and [11]. The advantage of using high-gain observers is that the control problem can be formulated in a standard singular perturbation format, and then the singular perturbation theory can be applied to analyze the closed-loop system stability. Moreover, when the speed of the high-gain observer is sufficiently high, the performance of the output feedback controller recovers the performance of the state feedback controller [14].

Adaptive control can handle not only parametric uncertainties but also dynamical uncertainties. To deal with dynamical uncertainties, different types of fixed-structure neural networks were used for function approximation. In [7] and [9], multilayer feedforward neural network-based adaptive robust control strategies were proposed. Compared with multilayer feedforward neural network, radial basis function (RBF) network [5], [8], [12], [13] is characterized by simpler structure, faster computation time, and superior adaptive performance. To apply fixed-structure neural networks for function approximation, the problem of structure determination has to be solved first. However, in general, it is impossible to know how to select the network parameters of fixed-structure neural networks at the beginning of the controller design process. Usually, they are determined offline by trial and error or using presumptive training data that may or may not be available. The problem of structure determination makes fixed-structure neural networks unsuitable for online applications.

Self-organizing approximation-based adaptive controllers were recently proposed for SISO feedback linearizable uncertain systems in [15]–[18]. In [15], a dynamic-structure RBF network that can grow was developed. In [16], a multilayer feedforward neural network with growing number of neurons was used. In [17], the local approximators based on locally weighted learning are augmented depending on the tracking performance. In [18], the resolution of the wavelet network can gradually increase according to the tracking performance and a dwell time constraint. Although the growing-structure approximation has been better than the fixed-structure approximation, it cannot prune the structures when they become redundant. As illustrated by simulations in [19], in the case when there are different control objectives, the existing RBFs that were added for the current control objective may become redundant for the next one. To alleviate this problem, variable-structure RBF networks that can both grow and shrink were considered in [19] and [20]. Variable-structure RBF networks preserve the advantages of RBF networks and, at the same time, overcome the limitations of fixed- and growing-structure RBF networks. However, the effect of the structure variation was not considered in the stability analysis therein.

In this paper, the output tracking control of a class of MIMO feedback linearizable uncertain systems is considered as in [9]–[12], where adaptive robust control strategies including both state and output feedback controllers

Manuscript received September 19, 2012; revised January 31, 2014 and May 20, 2014; accepted May 23, 2014.

J. Lian was with Purdue University, West Lafayette, IN 47907 USA. He is now with the Pacific Northwest National Laboratory, Richland, WA 99352 USA (e-mail: jianming.lian@pnnl.gov).

J. Hu and S. H. Żak are with the School of Electrical and Computer Engineering, Purdue University, West Lafayette, IN 47907 USA (e-mail: jianghai@ecn.purdue.edu; zak@purdue.edu).

Color versions of one or more of the figures in this paper are available online at http://ieeexplore.ieee.org.

Digital Object Identifier 10.1109/TNNLS.2014.2327853

are developed. The unknown system dynamics are approximated by a novel variable-structure RBF network that is improved from the self-organizing network used in [19] and [21]. The proposed RBF network avoids determining the network parameters offline by self-organizing the network structure online. It can add RBFs to improve the approximation accuracy when the tracking performance is poor. It can also remove RBFs to prevent the network redundancy when the tracking performance is satisfactory. To overcome the problem of fast switching between different structures in [19], a dwell time requirement on the structure variation similarly as in [18] and [22] is imposed. Due to the structure variation of the RBF network, the closed-loop system can be viewed as a switched system. Hence, the piecewise quadratic Lyapunov function [23], [24] is applied in the stability analysis to take into account the structure variation that was not considered in [19].

In summary, this paper has two major contributions: 1) a variable-structure RBF network is proposed as the self-organizing approximator, which can also be incorporated into existing fixed-structure neural network-based adaptive robust controllers, and 2) a switched system approach is proposed to analyze the system stability under variable-structure neural network-based adaptive robust controllers.

The remainder of this paper is organized as follows. The system description and the problem statement are given in Section II. In Section III, the variable-structure RBF network is described. In Section IV, an adaptive robust state feedback controller is developed, and then, in Section V, an adaptive robust output feedback controller is synthesized. In Section VI, the simulation results are included to illustrate the performance of the proposed variable neural adaptive robust controllers. The conclusion is given in Section VII.

II. System Description and Problem Statement

A. System Description

The class of uncertain systems considered herein consists of p coupled subsystems modeled by the set of equations

$$y_i^{(n_i)} = f_i(\boldsymbol{x}) + \sum_{j=1}^{p} g_{ij}(\boldsymbol{x})u_j + d_i, \quad i = 1, \ldots, p \tag{1}$$

where y_i, u_i, and d_i are the system output, system input and disturbance of the ith subsystem, respectively, and $f_i(\boldsymbol{x})$ and $g_{ij}(\boldsymbol{x})$ are unknown functions, where

$$\boldsymbol{x} = \left[y_1 \ \cdots \ y_1^{(n_1-1)} \ \cdots \ y_p \ \cdots \ y_p^{(n_p-1)} \right]^\top$$

is the state vector of the overall system. Let $(\boldsymbol{A}_i, \boldsymbol{b}_i)$ be a canonical controllable pair that represents a chain of n_i integrators, and let $\boldsymbol{c}_i = [1\ 0\ \cdots\ 0]_{1\times n_i}$, $\boldsymbol{y} = [y_1\ \cdots\ y_p]^\top$, $\boldsymbol{u} = [u_1\ \cdots\ u_p]^\top$, $\boldsymbol{d} = [d_1\ \cdots\ d_p]^\top$, $\boldsymbol{f}(\boldsymbol{x}) = [f_1(\boldsymbol{x})\ \cdots\ f_p(\boldsymbol{x})]^\top$, and $\boldsymbol{G}(\boldsymbol{x}) = [g_{ij}(\boldsymbol{x})]_{p\times p}$. Then, the uncertain system (1) can be represented in a compact form as

$$\begin{cases} \dot{\boldsymbol{x}} = \boldsymbol{A}\boldsymbol{x} + \boldsymbol{B}\left(\boldsymbol{f}(\boldsymbol{x}) + \boldsymbol{G}(\boldsymbol{x})\boldsymbol{u} + \boldsymbol{d}\right) \\ \boldsymbol{y} = \boldsymbol{C}\boldsymbol{x} \end{cases} \tag{2}$$

where $\boldsymbol{A} = \mathrm{diag}[\boldsymbol{A}_1\ \cdots\ \boldsymbol{A}_p]$, $\boldsymbol{B} = \mathrm{diag}[\boldsymbol{b}_1\ \cdots\ \boldsymbol{b}_p]$, and $\boldsymbol{C} = \mathrm{diag}[\boldsymbol{c}_1\ \cdots\ \boldsymbol{c}_p]$. The above system is often referred to as a square system because the number of inputs and the number of outputs are the same.

Assumption 1: The function $\boldsymbol{f}(\boldsymbol{x})$ and $\boldsymbol{G}(\boldsymbol{x})$ are Lipschitz continuous in $\boldsymbol{x}$.

Assumption 2: The function $\boldsymbol{G}(\boldsymbol{x})$ is uniformly definite. Without loss of generality, it is assumed that $\boldsymbol{G}(\boldsymbol{x})$ is uniformly positive definite with $\|\boldsymbol{G}(\boldsymbol{x})\| \geq \underline{g} > 0$, where $\underline{g}$ is a known constant and $\|\cdot\|$ denotes the Euclidean norm.

Assumption 3: The disturbance $\boldsymbol{d}$ is a lumped term of unmodeled system dynamics and external disturbances. It is Lipschitz continuous in $\boldsymbol{x}$ and piecewise continuous in t. In addition, it is globally bounded, that is, $\|\boldsymbol{d}\| \leq d_o$, where d_o is a known positive constant.

It was pointed out in [10] that many physical systems, such as natural Lagrangian systems and circuit systems, can be modeled in the form of (1). The current-controlled three-phase epoxy core linear described in [25] and the planar articulated two-link manipulator given in [26] are both examples.

B. Problem Statement

Our objective is to develop a tracking control strategy such that the ith system output y_i, $i = 1, \ldots, p$, tracks a reference signal y_{di}. It is assumed that y_{di} has bounded derivatives up to the n_ith order, that is, $y_{di}^{(n_i)} \in \Omega_{y_{di}}$, where $\Omega_{y_{di}} \subset \mathbb{R}$ is a compact set. Let $\boldsymbol{y}_d^{(n)} = [y_{d1}^{(n_1)}\ \cdots\ y_{dp}^{(n_p)}]^\top$. Then, $\boldsymbol{y}_d^{(n)} \in \boldsymbol{\Omega}_{y_d}$, where $\boldsymbol{\Omega}_{y_d} \subset \mathbb{R}^p$ is a compact set. Define the desired system state vector as $\boldsymbol{x}_d = [y_{d1}\ \cdots\ y_{d1}^{(n_1-1)}\ \cdots\ y_{dp}\ \cdots\ y_{dp}^{(n_p-1)}]^\top$. Then, $\boldsymbol{x}_d \in \boldsymbol{\Omega}_{x_d}$, where $\boldsymbol{\Omega}_{x_d}$ is a compact subset of $\mathbb{R}^n$ with $n = \sum_{i=1}^{p} n_i$. Let $e_{yi} = y_i - y_{di}$ denote the ith output tracking error. Define the output tracking error as $\boldsymbol{e}_y = [e_{y1}\ \cdots\ e_{yp}]^\top$ and the state tracking error as

$$\boldsymbol{e} = \boldsymbol{x} - \boldsymbol{x}_d. \tag{3}$$

Then, $\boldsymbol{e} = [\boldsymbol{e}_1^\top\ \cdots\ \boldsymbol{e}_p^\top]^\top$, where $\boldsymbol{e}_i = [e_{yi}\ \cdots\ e_{yi}^{(n_i-1)}]^\top$. It follows from (2) that

$$\dot{\boldsymbol{e}} = \boldsymbol{A}\boldsymbol{e} + \boldsymbol{B}\big(\boldsymbol{f}(\boldsymbol{x}) + \boldsymbol{G}(\boldsymbol{x})\boldsymbol{u} - \boldsymbol{y}_d^{(n)} + \boldsymbol{d}\big). \tag{4}$$

Our goal is to design the control input $\boldsymbol{u}$ so that the state tracking error can be as small as possible.

Let $\hat{\boldsymbol{f}}(\boldsymbol{x})$ and $\hat{\boldsymbol{G}}(\boldsymbol{x})$ be approximations of $\boldsymbol{f}(\boldsymbol{x})$ and $\boldsymbol{G}(\boldsymbol{x})$, respectively, where $\hat{\boldsymbol{G}}(\boldsymbol{x})$ is invertible. Consider the controller of the following form,

$$\boldsymbol{u} = \boldsymbol{u}_a = \hat{\boldsymbol{G}}^{-1}(\boldsymbol{x})\big(-\hat{\boldsymbol{f}}(\boldsymbol{x}) + \boldsymbol{y}_d^{(n)} - \boldsymbol{K}\boldsymbol{e}\big) \tag{5}$$

where $\boldsymbol{K} = \mathrm{diag}[\boldsymbol{k}_1\ \cdots\ \boldsymbol{k}_p]$ is selected such that $\boldsymbol{A}_{mi} = \boldsymbol{A}_i - \boldsymbol{b}_i\boldsymbol{k}_i$ is Hurwitz. Applying the controller defined in (5) to the state tracking error dynamics (4), it gives the following after several manipulations,

$$\dot{\boldsymbol{e}} = \boldsymbol{A}_m\boldsymbol{e} + \boldsymbol{B}\big(\boldsymbol{f}(\boldsymbol{x}) - \hat{\boldsymbol{f}}(\boldsymbol{x}) + \big(\boldsymbol{G}(\boldsymbol{x}) - \hat{\boldsymbol{G}}(\boldsymbol{x})\big)\boldsymbol{u}_a + \boldsymbol{d}\big) \tag{6}$$

where $\boldsymbol{A}_m = \mathrm{diag}[\boldsymbol{A}_{m1}\ \cdots\ \boldsymbol{A}_{mp}]$ is Hurwitz. The state tracking error of the closed-loop system driven by $\boldsymbol{u}_a$ will not, in general, converge to zero due to the presence of estimation errors and disturbances. Therefore, a robustifying component

is also required to ensure a desired tracking performance. On the other hand, to guarantee the existence of $\boldsymbol{u}_a$ given by (5), it requires that $\hat{\boldsymbol{G}}(\boldsymbol{x})$ be always nonsingular. The problem caused by the singularity of $\hat{\boldsymbol{G}}(\boldsymbol{x})$ generated by neural network is referred to as stabilizability problem in [12]. Therefore, this problem has to be resolved first in the controller design process for (1). In [10] and [11], $\hat{\boldsymbol{G}}(\boldsymbol{x})$ was assumed to be nonsingular. In [9], restrictive assumptions were imposed on the parameter vectors of the multilayer feedforward networks to guarantee that $\hat{\boldsymbol{G}}(\boldsymbol{x})$ is invertible. The attempt to solve this problem was first reported in [12] in the design of robust adaptive state feedback controller.

In the following controller designs, a variable-structure RBF network that is described in the next section is first proposed to approximate the unknown function $\boldsymbol{f}(\boldsymbol{x})$. A constant positive definite matrix $\boldsymbol{G}_0$ is used instead of the proposed variable-structure RBF network to approximate the unknown function $\boldsymbol{G}(\boldsymbol{x})$, that is, $\hat{\boldsymbol{G}}(\boldsymbol{x}) = \boldsymbol{G}_0$.

III. Variable-Structure RBF Network

The variable-structure RBF network used to approximate $\boldsymbol{f}(\boldsymbol{x})$ over a compact set $\boldsymbol{\Omega}_x$ is an improved version of the self-organizing RBF network in [19], which, in turn, was adopted from [21]. The proposed variable-structure RBF network can have N different possible structures, where N is determined by the design parameters discussed later. For each structure, the RBF network consists of n input neurons, M_υ hidden neurons, where $\upsilon \in \{1, \ldots, N\}$ denotes the scalar index, and p output neurons. The kth output of the RBF network with the υth possible structure can be represented as

$$\hat{f}_{k,\upsilon}(\boldsymbol{x}) = \sum_{j=1}^{M_\upsilon} \omega_{kj,\upsilon}\xi_{j,\upsilon}(\boldsymbol{x}) = \sum_{j=1}^{M_\upsilon} \omega_{kj,\upsilon} \prod_{i=1}^{n} \psi\left(\frac{|x_i - c_{ij,\upsilon}|}{\delta_{ij,\upsilon}}\right) \tag{7}$$

where $\omega_{kj,\upsilon}$ is the weight from the jth hidden neuron to the kth output neuron and $\xi_{j,\upsilon}(\boldsymbol{x})$ is the RBF for the jth hidden neuron. The parameter $c_{ij,\upsilon}$ is the ith coordinate of the center of $\xi_{j,\upsilon}(\boldsymbol{x})$, $\delta_{ij,\upsilon}$ is the radius of $\xi_{j,\upsilon}(\boldsymbol{x})$ in the ith coordinate, and $\psi : [0, \infty) \to \mathbb{R}^+$ is the activation function. Let $\boldsymbol{W}_\upsilon = [\boldsymbol{\omega}_{1,\upsilon} \ \cdots \ \boldsymbol{\omega}_{p,\upsilon}]$ with $\boldsymbol{\omega}_{i,\upsilon} = [\omega_{i1,\upsilon} \ \cdots \ \omega_{iM_\upsilon,\upsilon}]^\top$ and $\boldsymbol{\xi}_\upsilon(\boldsymbol{x}) = [\xi_{1,\upsilon}(\boldsymbol{x}) \ \cdots \ \xi_{M_\upsilon,\upsilon}(\boldsymbol{x})]^\top$. Then

$$\hat{\boldsymbol{f}}_\upsilon(\boldsymbol{x}) = \boldsymbol{W}_\upsilon^\top \boldsymbol{\xi}_\upsilon(\boldsymbol{x}).$$

The raised-cosine RBF (RCRBF) proposed in [27] is employed instead of the commonly used Gaussian RBF because the compact support of the RCRBF enables fast and efficient training and output evaluation of the RBF network. The 1-D RCRBF is defined as

$$\psi(x) = \begin{cases} \frac{1}{2}\left(1 + \cos\left(\frac{\pi(x-c)}{\delta}\right)\right) & \text{if } |x - c| \le \delta \\ 0 & \text{if } |x - c| > \delta \end{cases}$$

where c is the center and δ is the radius. The n-dimensional RCRBF can be represented as the product of n 1-D RCRBFs.

In the following sections, a detailed description of the improved variable-structure RBF network is provided. The major improvement over [19] lies in the RBF adding and removing operations. Moreover, a dwell time T_d, which is a design parameter, is introduced into the structure variation of the RBF network to prevent excessively fast switching between different structures. Under the dwell time requirement, the network has to stay with the current structure for the duration of at least T_d before switching to a different structure.

A. Center Grid

Recall that the unknown function $\boldsymbol{f}(\boldsymbol{x})$ is approximated over a compact set $\boldsymbol{\Omega}_x \subset \mathbb{R}^n$. Without loss of generality, it is assumed that $\boldsymbol{\Omega}_x$ has the form

$$\boldsymbol{\Omega}_x = \left\{\boldsymbol{x} \in \mathbb{R}^n : \boldsymbol{x}_l \le \boldsymbol{x} \le \boldsymbol{x}_u\right\}$$

where the n-dimensional vectors $\boldsymbol{x}_l = [x_{l1} \ \cdots \ x_{ln}]^\top$ and $\boldsymbol{x}_u = [x_{u1} \ \cdots \ x_{un}]^\top$ denote lower and upper bounds of the components of $\boldsymbol{x}$, respectively. To represent the centers of the RBFs inside the approximation region, an n-dimensional center grid with layer hierarchy is used, where each grid node corresponds to one RBF. This n-dimensional center grid can be mathematically described by $S_1 \times \cdots \times S_n$, where S_i is the location set in the ith coordinate and the symbol $\times$ denotes the Cartesian product. The center grid is initialized inside the approximation region $\boldsymbol{\Omega}_x$ with $S_i = \{x_{li}, x_{ui}\}$, $i = 1, \ldots, n$. The 2^n grid nodes of the initial grid are referred to as boundary grid nodes, and cannot be removed. In each coordinate, additional locations can be added, and then may be removed from S_i as the controlled system evolves in time. However, new grid nodes can only be added at positions determined coordinate-wise by potential locations. In each coordinate, the potential locations are equally spaced. The first layer contains two fixed boundary locations. The second layer has only one potential location in the middle of the boundary locations. Then, the potential locations of the subsequent layers are in the middle of the adjacent potential locations of all the previous layers.

B. Adding RBFs

The network can add new RBFs, that is, new grid nodes to improve approximation accuracy, if the following conditions are satisfied:

1) the elapsed time since the last operation of either adding or removing is greater than the dwell time T_d;
2) $\|\boldsymbol{e}_y\| > e_{\max}$, where $e_{\max}$ is a prespecified design parameter, for a period of time greater than T_d.

First, the nearest neighboring grid node in the center grid to the current input $\boldsymbol{x}$ is located among existing grid nodes, which is denoted by $\boldsymbol{c}_{(\text{nearest})}$. Then, the nearer neighboring grid node denoted by $\boldsymbol{c}_{(\text{nearer})}$ is located, where each element of $\boldsymbol{c}_{(\text{nearer})}$, that is, $c_{i(\text{nearer})}$, is determined such that x_i is between $c_{i(\text{nearest})}$ and $c_{i(\text{nearer})}$. Next, the adding operation is performed for each coordinate independently. In the ith coordinate, if the following conditions are satisfied:

3) $|x_i - c_{i(\text{nearest})}| > \frac{1}{4}|c_{i(\text{nearest})} - c_{i(\text{nearer})}|$;
4) $|x_i - c_{i(\text{nearest})}| > d_{i(\text{threshold})}$, where $d_{i(\text{threshold})}$ is a design parameter that specifies the minimum grid distance in the ith coordinate, and thus determines the number of admissible structures denoted by N.

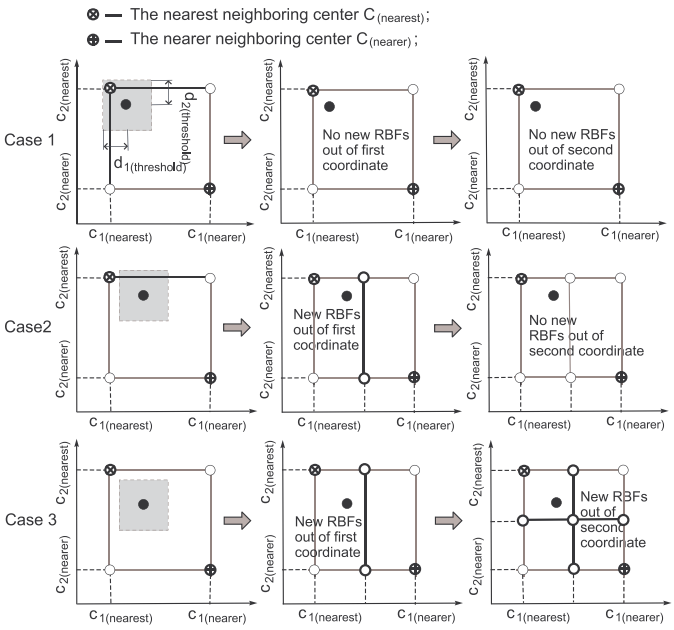

Fig. 1. 2-D examples of adding RBFs.

A new location at the half of the sum of $c_{i(\text{nearest})}$ and $c_{i(\text{nearer})}$ is added into S_i. Otherwise, no new location is added to S_i. The layer of the newly added location is one level higher than the highest layer of the two adjacent existing locations in the same coordinate. The operation of adding RBFs is illustrated with 2-D examples shown in Fig. 1.

Remark 1: The design parameter $e_{\max}$ plays an important role in determining whether the RBF network keeps switching between different structures all the time or not. It should be appropriately selected to account for the effects of residual disturbances. If $e_{\max}$ is chosen to be very small, the neural network could keep changing its structure by adding more RBFs even though the output tracking error has already been within the acceptable range. In such a case, the neural network will eventually fit to residual disturbances.

C. Removing RBFs

The network can remove some of the existing RBFs, that is, some of the existing grid nodes to prevent network redundancy, if the following conditions are satisfied:

1) the elapsed time since the last operation of either adding or removing is greater than the dwell time T_d;
2) $\|\boldsymbol{e}_y\| \le \rho e_{\max}$, where $\rho \in (0, 1]$, for a period of time greater than T_d.

First, the nearest and the nearer neighboring grid nodes in the center grid, $\boldsymbol{c}_{(\text{nearest})}$ and $\boldsymbol{c}_{(\text{nearer})}$, to the current input $\boldsymbol{x}$ are located. Then, the RBF removing operation is implemented for each coordinate independently. In the ith coordinate, if the following conditions are satisfied:

3) $c_{i(\text{nearest})} \notin \{x_{li}, x_{ui}\}$;
4) the location $c_{i(\text{nearest})}$ is in the higher or the same layer as the highest layer of the two neighboring locations in the same coordinate;
5) $|x_i - c_{i(\text{nearest})}| < \varrho |c_{i(\text{nearest})} - c_{i(\text{nearer})}|$, where $\varrho \in (0, 0.5)$,

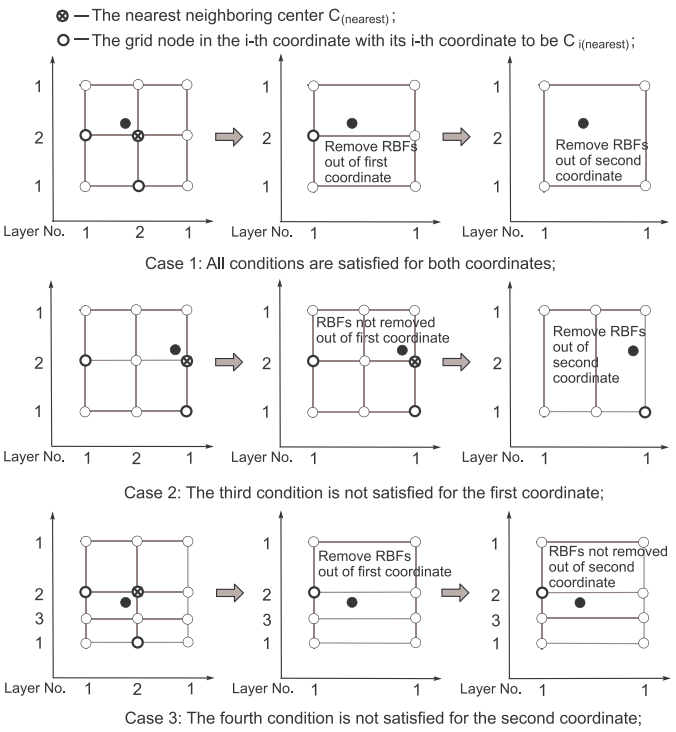

Fig. 2. 2-D examples of removing RBFs.

then the location $c_{i(\text{nearest})}$ is removed from S_i. Otherwise, no location is removed from S_i. 2-D examples of removing RBFs are given in Fig. 2.

Remark 2: Before the system reaches the steady state, the transients reflected within $\boldsymbol{e}_y$ will cause the RBF network to add many unnecessary RBFs through. This is the disadvantage of existing variable-structure RBF networks in the literature whose sizes can only grow. It is desirable to have the RBF removing operation that will remove those unnecessary RBFs later in the steady state. Thus, the main feature of the proposed variable-structure RBF network herein is the vital capability of removing RBFs in addition to adding RBFs.

D. Uniform Grid Transformation

The determination of the radius of the RBF is much easier in a uniform grid than in a nonuniform grid because the RBF is radially symmetric with respect to its center. However, the center grid used to locate RBFs is usually nonuniform. In addition, the structure of the center grid changes after each adding or removing operation, which further complicates the problem. To simplify the process of determination of the radius, the one-to-one mapping $\boldsymbol{z}(\boldsymbol{x}) = [z_1(x_1) \ \cdots \ z_n(x_n)]^\top$, proposed in [27], is used to transform the center grid into a uniform grid. Suppose that the RBF network assumes the υth possible structure after the adding or removing operation and there are $M_{i,\upsilon}$ distinct elements in S_i ordered as $c_{i(1)} < \cdots < c_{i(M_{i,\upsilon})}$, where $c_{i(k)}$ is the kth element with $c_{i(1)} = x_{li}$ and $c_{i(M_{i,\upsilon})} = x_{ui}$. Then, the mapping function $z_i(x_i) : [x_{li}, x_{ui}] \to [1, M_{i,\upsilon}]$ takes the form

$$z_i(x_i) = k + \frac{x_i - c_{i(k)}}{c_{i(k+1)} - c_{i(k)}}, \quad c_{i(k)} \le x_i < c_{i(k+1)} \tag{8}$$

which maps $c_{i(k)}$ into the integer k. Thus, the transformation $\boldsymbol{z}(\boldsymbol{x}) : \boldsymbol{\Omega}_x \to \mathbb{R}^n$ maps the center grid into a grid with unit

spacing between adjacent grid nodes such that the radius of the RBF can be easily chosen. For the RCRBF, the radius in every coordinate is selected to be equal to one unit, that is, the radius will touch but not extend beyond the neighboring grid nodes in the uniform grid. This particular choice guarantees that for any given input $\boldsymbol{x}$, the number of nonzero RCRBFs in the uniform grid is at most 2^n.

To simplify the implementation, let the vector $\boldsymbol{q}_\upsilon \in \mathbb{R}^n$ be the index vector of the grid nodes, where $\boldsymbol{q}_\upsilon = [q_{1,\upsilon} \ \cdots \ q_{n,\upsilon}]^\top$ with $1 \le q_{i,\upsilon} \le M_{i,\upsilon}$. Then, the scalar index j can be uniquely determined by the index vector $\boldsymbol{q}_\upsilon$, where

$$j = (q_{n,\upsilon} - 1)M_{n-1,\upsilon} \cdots M_{2,\upsilon} M_{1,\upsilon} + \cdots + (q_{3,\upsilon} - 1)M_{2,\upsilon} M_{1,\upsilon} + (q_{2,\upsilon} - 1)M_{1,\upsilon} + q_{1,\upsilon}. \quad (9)$$

Let $\boldsymbol{c}_{j,\upsilon} = [c_{1j,\upsilon} \ \cdots \ c_{nj,\upsilon}]^\top$ denote the location of the $\boldsymbol{q}_\upsilon$th grid node in the original grid. Then, the corresponding grid node in the uniform grid is located at $\boldsymbol{z}_{j,\upsilon} = \boldsymbol{z}(\boldsymbol{c}_{j,\upsilon}) = [q_{1,\upsilon} \ \cdots \ q_{n,\upsilon}]^\top$. Using the scalar index j in (9), the output $\hat{f}_{i,\upsilon}(\boldsymbol{x})$ of the variable-structure RCRBF network implemented in the uniform grid can be expressed as

$$\hat{f}_{i,\upsilon}(\boldsymbol{x}) = \sum_{j=1}^{M_\upsilon} \omega_{ij,\upsilon} \xi_{j,\upsilon}(\boldsymbol{x}) = \sum_{j=1}^{M_\upsilon} \omega_{ij,\upsilon} \prod_{i=1}^{n} \psi\left(|z_i(x_i) - q_{i,\upsilon}|\right) \quad (10)$$

where the radius is one unit in each coordinate.

When implementing the output feedback controller, the state vector estimate $\hat{\boldsymbol{x}}$ is used rather than the actual state vector $\boldsymbol{x}$. It may happen that $\hat{\boldsymbol{x}} \notin \boldsymbol{\Omega}_x$. In such a case, the definition of the transformation (8) is extended as

$$\begin{cases} z_i(\hat{x}_i) = 1 & \text{if } \hat{x}_i < c_{i(1)} \\ z_i(\hat{x}_i) = M_{i,\upsilon} & \text{if } \hat{x}_i > c_{i(M_{i,\upsilon})} \end{cases} \quad (11)$$

for $i = 1, \ldots, n$. If $\hat{\boldsymbol{x}} \in \boldsymbol{\Omega}_x$, the transformation (8) is used. Therefore, it follows from (8) and (11) that the function $\boldsymbol{z}(\boldsymbol{x})$ maps the whole n-dimensional space $\mathbb{R}^n$ into the compact set $[1, M_{1,\upsilon}] \times [1, M_{2,\upsilon}] \times \cdots \times [1, M_{n,\upsilon}]$.

IV. State Feedback Controller Development

The proposed adaptive robust state feedback controller is

$$\boldsymbol{u} = \boldsymbol{u}_{a,\upsilon} + \boldsymbol{u}_{s,\upsilon} \quad (12)$$

where

$$\boldsymbol{u}_{a,\upsilon} = \boldsymbol{G}_0^{-1}\big(- \hat{\boldsymbol{f}}_\upsilon(\boldsymbol{x}) + \boldsymbol{y}_d^{(n)} - \boldsymbol{K}\boldsymbol{e}\big)$$

with $\hat{\boldsymbol{f}}_\upsilon(\boldsymbol{x}) = \boldsymbol{W}_\upsilon^\top \boldsymbol{\xi}_\upsilon(\boldsymbol{x})$ and $\boldsymbol{u}_{s,\upsilon}$ is the robustifying component described later. Note that the architecture of the above controller varies as the structure of the RBF network changes. A particular controller architecture is referred to as a mode. Because there are N possible network structures, the proposed controller has N different modes. Let $\boldsymbol{\Omega}_{e_0}$ be a compact set that contains all possible initial state tracking errors and let $c_{e_0} = \max_{\boldsymbol{e} \in \boldsymbol{\Omega}_{e_0}} \frac{1}{2}\boldsymbol{e}^\top \boldsymbol{P}_m \boldsymbol{e}$, where $\boldsymbol{P}_m = \text{diag}[\boldsymbol{P}_{m1} \ \cdots \ \boldsymbol{P}_{mp}]$ is the solution to the continuous Lyapunov matrix equation $\boldsymbol{A}_m^\top \boldsymbol{P}_m + \boldsymbol{P}_m \boldsymbol{A}_m = -2\boldsymbol{Q}_m$ for $\boldsymbol{Q}_m = \text{diag}[\boldsymbol{Q}_{m1} \ \cdots \ \boldsymbol{Q}_{mp}]$ with $\boldsymbol{Q}_{mi} = \boldsymbol{Q}_{mi}^\top > 0$.

Definition 1: The compact set $\boldsymbol{\Omega}_x$ is defined as

$$\boldsymbol{\Omega}_x = \big\{\boldsymbol{x} : \boldsymbol{x} = \boldsymbol{e} + \boldsymbol{x}_d, \boldsymbol{e} \in \boldsymbol{\Omega}_e, \boldsymbol{x}_d \in \boldsymbol{\Omega}_{x_d}\big\}$$

where $\boldsymbol{\Omega}_e = \{\boldsymbol{e} : \frac{1}{2}\boldsymbol{e}^\top \boldsymbol{P}_m \boldsymbol{e} \le c_e\}$ with $c_e > c_{e_0}$.

Remark 3: In the literature, it is common to assume that the compact set $\boldsymbol{\Omega}_x$ is large enough but not given explicitly. In this paper, the compact set $\boldsymbol{\Omega}_x$ above is defined by two known compact sets $\boldsymbol{\Omega}_{x_d}$ and $\boldsymbol{\Omega}_e$. The compact set $\boldsymbol{\Omega}_{x_d}$ is determined by the range of bounded reference signals and their bounded derivatives up to the n_ith order. On the other hand, the compact set $\boldsymbol{\Omega}_e$ is selected to contain the initial tracking error. The control strategies proposed in this paper guarantee that $\boldsymbol{x}(t)$ is confined in the compact set $\boldsymbol{\Omega}_x$.

Definition 2: The compact set $\boldsymbol{\Omega}_{i,\upsilon}$ is defined as

$$\boldsymbol{\Omega}_{i,\upsilon} = \big\{\boldsymbol{\omega}_{i,\upsilon} : \underline{\omega}_i \le \omega_{ij,\upsilon} \le \overline{\omega}_i, 1 \le j \le M_\upsilon\big\}$$

where the lower and the upper bounds $\underline{\omega}_i$ and $\overline{\omega}_i$, $i = 1, \ldots, p$, are design parameters.

To proceed, the weight vectors $\boldsymbol{\omega}_{i,\upsilon}$ are constrained to reside inside $\boldsymbol{\Omega}_{i,\upsilon}$. Let $\boldsymbol{W}_\upsilon^* = [\boldsymbol{\omega}_{1,\upsilon}^* \ \cdots \ \boldsymbol{\omega}_{p,\upsilon}^*]$ denote the optimal constant weight matrix corresponding to each possible network structure. This optimal weight matrix is used only in the analytical analysis, and is defined as

$$\boldsymbol{W}_\upsilon^* = \underset{\boldsymbol{\omega}_{i,\upsilon} \in \boldsymbol{\Omega}_{i,\upsilon}}{\text{argmin}} \max_{\boldsymbol{x} \in \boldsymbol{\Omega}_x} \big\| \boldsymbol{f}(\boldsymbol{x}) - \boldsymbol{W}_\upsilon^\top \boldsymbol{\xi}_\upsilon(\boldsymbol{x}) \big\|.$$

Let

$$\boldsymbol{\Phi}_\upsilon = \boldsymbol{W}_\upsilon - \boldsymbol{W}_\upsilon^*. \quad (13)$$

Then, $\boldsymbol{\Phi}_\upsilon = [\boldsymbol{\phi}_{1,\upsilon} \ \cdots \ \boldsymbol{\phi}_{p,\upsilon}]$, where $\boldsymbol{\phi}_{i,\upsilon} = \boldsymbol{\omega}_{i,\upsilon} - \boldsymbol{\omega}_{i,\upsilon}^*$. Let $c = \sum_{i=1}^p c_i$, where

$$c_i = \max_\upsilon \left(\max_{\boldsymbol{\omega}_{i,\upsilon}, \boldsymbol{\omega}_{i,\upsilon}^* \in \boldsymbol{\Omega}_{i,\upsilon}} \frac{1}{2\kappa} \boldsymbol{\phi}_{i,\upsilon}^\top \boldsymbol{\phi}_{i,\upsilon} \right) \quad (14)$$

and where $\kappa > 0$ is a design parameter, and $\max_\upsilon(\cdot)$ denotes the maximization taken over all the potential structures of the RBF networks. It is obvious that c_i decreases as κ increases. Let $\boldsymbol{\sigma} = \boldsymbol{B}^\top \boldsymbol{P}_m \boldsymbol{e}$. The following projection-based weight matrix adaptation law is employed,

$$\dot{\boldsymbol{W}}_\upsilon = \text{Proj}\left(\boldsymbol{W}_\upsilon, \kappa \boldsymbol{\xi}_\upsilon(\boldsymbol{x}) \boldsymbol{\sigma}^\top\right) \quad (15)$$

where $\text{Proj}(\boldsymbol{W}_\upsilon, \boldsymbol{\Theta}_\upsilon)$ denotes $\text{Proj}(\omega_{ij,\upsilon}, \theta_{ij,\upsilon})$, $i = 1, \ldots, p$ and $j = 1, \ldots, M_\upsilon$. Then, the projection operator as proposed in [28] is used

$$\text{Proj}(\omega_{ij,\upsilon}, \theta_{ij,\upsilon}) = \begin{cases} 0 & \text{if } \omega_{ij,\upsilon} = \underline{\omega}_i \text{ and } \theta_{ij,\upsilon} < 0 \\ 0 & \text{if } \omega_{ij,\upsilon} = \overline{\omega}_i \text{ and } \theta_{ij,\upsilon} > 0 \\ \theta_{ij,\upsilon} & \text{otherwise} \end{cases}$$

which guarantees that $\boldsymbol{\omega}_{i,\upsilon}(t) \in \boldsymbol{\Omega}_{i,\upsilon}$ for $t \ge t_0$ if $\boldsymbol{\omega}_{i,\upsilon}(t_0) \in \boldsymbol{\Omega}_{i,\upsilon}$. It follows from the definition of the projection operator that $\boldsymbol{\phi}_{i,\upsilon}^\top \left(\dot{\boldsymbol{\omega}}_{i,\upsilon} - \boldsymbol{\theta}_{i,\upsilon}\right) \le 0$, which implies that

$$\frac{1}{\kappa} \text{trace}\left(\boldsymbol{\Phi}_\upsilon^\top \left(\dot{\boldsymbol{W}}_\upsilon - \kappa \boldsymbol{\xi}_\upsilon(\boldsymbol{x}) \boldsymbol{\sigma}^\top\right)\right) \le 0. \quad (16)$$

Applying the proposed adaptive robust state feedback controller given by (12) to the state tracking error dynamics (4), it gives the following after several manipulations,

$$\begin{aligned} \dot{\boldsymbol{e}} &= \boldsymbol{A}\boldsymbol{e} + \boldsymbol{B}\big(\boldsymbol{f}(\boldsymbol{x}) + \boldsymbol{G}(\boldsymbol{x})\boldsymbol{u}_{a,\upsilon} + \boldsymbol{G}(\boldsymbol{x})\boldsymbol{u}_{s,\upsilon} - \boldsymbol{y}_d^{(n)} + \boldsymbol{d}\big) \\ &= \boldsymbol{A}_m \boldsymbol{e} - \boldsymbol{B}\boldsymbol{\Phi}_\upsilon^\top \boldsymbol{\xi}_\upsilon(\boldsymbol{x}) + \boldsymbol{B}\big(\boldsymbol{G}(\boldsymbol{x}) - \boldsymbol{G}_0\big)\boldsymbol{u}_{a,\upsilon} + \boldsymbol{B}\boldsymbol{d} \\ &\quad + \boldsymbol{B}\boldsymbol{G}(\boldsymbol{x})\boldsymbol{u}_{s,\upsilon} + \boldsymbol{B}\big(\boldsymbol{f}(\boldsymbol{x}) - \boldsymbol{W}_\upsilon^{*\top} \boldsymbol{\xi}_\upsilon(\boldsymbol{x})\big). \end{aligned} \quad (17)$$

As can be seen from (17), the robustifying component $\boldsymbol{u}_{s,\upsilon}$ has to counteract the effects of the approximation error as well as the bounded disturbance to force the state tracking error $\boldsymbol{e}$ converge or, at least, be bounded.

Definition 3: The positive constants d_f^* and d_g^* are defined, respectively, as the optimal approximation errors

$$d_f^* = \max_{\upsilon} \left(\max_{\boldsymbol{x} \in \boldsymbol{\Omega}_x} \left\| \boldsymbol{f}(\boldsymbol{x}) - \boldsymbol{W}_\upsilon^{*\top} \boldsymbol{\xi}_\upsilon(\boldsymbol{x}) \right\| \right)$$

and $d_g^* = \max_{\boldsymbol{x} \in \boldsymbol{\Omega}_x} \|\boldsymbol{G}(\boldsymbol{x}) - \boldsymbol{G}_0\|$.

Assumption 4: The optimal approximation errors d_f^* and d_g^* are known nonnegative constants.

The robustifying component $\boldsymbol{u}_{s,\upsilon}$ is proposed to be

$$\boldsymbol{u}_{s,\upsilon} = \begin{cases} -\dfrac{k_{s,\upsilon}}{\underline{g}} \dfrac{\boldsymbol{\sigma}}{\|\boldsymbol{\sigma}\|} & \text{if } \|\boldsymbol{\sigma}\| \geq \nu \\ -\dfrac{k_{s,\upsilon}}{\underline{g}} \dfrac{\boldsymbol{\sigma}}{\nu} & \text{if } \|\boldsymbol{\sigma}\| < \nu \end{cases} \tag{18}$$

where $\nu > 0$ is a design parameter, and $k_{s,\upsilon} = d_f + d_g \|\boldsymbol{u}_{a,\upsilon}\| + d_o$ with $d_f \geq d_f^*$ and $d_g \geq d_g^*$.

Remark 4: In the case when the optimal approximation errors d_f^* and d_g^* are not available, if $\|\boldsymbol{f}(\boldsymbol{x})\| \leq \overline{f}$ and $\|\boldsymbol{G}(\boldsymbol{x})\| \leq \overline{g}$ with known $\overline{f}$ and $\overline{g}$, one can conservatively choose $d_f = \overline{d}_f$ and $d_g = \overline{d}_g$, where

$$\overline{d}_f = \overline{f} + \max_{\upsilon} \left(\max_{\boldsymbol{\omega}_{i,\upsilon} \in \boldsymbol{\Omega}_{i,\upsilon}, \boldsymbol{x} \in \boldsymbol{\Omega}_x} \left\| \boldsymbol{W}_\upsilon{}^\top \boldsymbol{\xi}_\upsilon(\boldsymbol{x}) \right\| \right) \geq d_f^*$$

and $\overline{d}_g = \overline{g} + \|\boldsymbol{G}_0\| \geq d_g^*$. Therefore, the necessary assumption for the proposed adaptive robust controller design is that the bounds of the unknown functions $\boldsymbol{f}(\boldsymbol{x})$ and $\boldsymbol{G}(\boldsymbol{x})$ are known, which is reasonable from a practical point of view and has been commonly used in the literature.

Remark 5: Let the increasing sequence $\{t_i\}_{i=0}^{\infty}$ be a partition of the interval $[t_0, \infty)$ such that $\upsilon = \upsilon_i$ over $[t_i, t_{i+1})$. During the ith time interval $[t_i, t_{i+1})$, the controller $\boldsymbol{u}$ given by (12) and (18) has a fixed architecture. Thus, as discussed in [29], there exists a unique solution $\boldsymbol{x}_{\upsilon_i}(t)$ to (2) starting at $\boldsymbol{x}_{\upsilon_i}(t_i)$ over $[t_i, t_{i+1})$. On the other hand, the dwell time requirement on each mode has been imposed so that $t_{i+1} - t_i \geq T_d$. Therefore, the solutions $\boldsymbol{x}_{\upsilon_i}(t)$ over $[t_i, t_{i+1})$ can be pieced together to establish the existence of a unique solution $\boldsymbol{x}(t)$ to (2) starting at $\boldsymbol{x}(t_0)$ over $[t_0, \infty)$, where $\boldsymbol{x}_{\upsilon_0}(t_0) = \boldsymbol{x}(t_0)$ and $\boldsymbol{x}_{\upsilon_{i+1}}(t_{i+1}) = \boldsymbol{x}_{\upsilon_i}(t_{i+1}^-)$. Here, $\boldsymbol{x}_{\upsilon_i}(t_{i+1}^-) = \lim_{t \to t_{i+1}^-} x_{\upsilon_i}(t)$.

Now, consider the piecewise quadratic Lyapunov function whenever the proposed controller (12) is in the υth mode

$$V_\upsilon = \frac{1}{2} \boldsymbol{e}^\top \boldsymbol{P}_m \boldsymbol{e} + \frac{1}{2\kappa} \operatorname{trace}\left(\boldsymbol{\Phi}_\upsilon^\top \boldsymbol{\Phi}_\upsilon \right) \tag{19}$$

where $\boldsymbol{e}$ and $\boldsymbol{\Phi}_\upsilon$ are defined in (3) and (13), respectively. This Lyapunov function has jump discontinuities when the proposed controller switches between different modes. Evaluating the time derivative of V_υ on the solutions of (17) and taking into account (16), it gives

$$\begin{aligned} \dot{V}_\upsilon &= \boldsymbol{e}^\top \boldsymbol{P}_m \dot{\boldsymbol{e}} + \frac{1}{\kappa} \operatorname{trace}\left(\boldsymbol{\Phi}_\upsilon^\top \dot{\boldsymbol{\Phi}}_\upsilon \right) \\ &= -\boldsymbol{e}^\top \boldsymbol{Q}_m \boldsymbol{e} + \boldsymbol{\sigma}^\top \boldsymbol{G}(\boldsymbol{x}) \boldsymbol{u}_{s,\upsilon} + \boldsymbol{\sigma}^\top \big(\boldsymbol{G}(\boldsymbol{x}) - \boldsymbol{G}_0 \big) \boldsymbol{u}_{a,\upsilon} \\ &\quad + \boldsymbol{\sigma}^\top \big(\boldsymbol{f}(\boldsymbol{x}) - \boldsymbol{W}_\upsilon^{*\top} \boldsymbol{\xi}_\upsilon(\boldsymbol{x}) \big) + \boldsymbol{\sigma}^\top \boldsymbol{d} \\ &\quad + \frac{1}{\kappa} \operatorname{trace}\left(\boldsymbol{\Phi}_\upsilon^\top \dot{\boldsymbol{\Phi}}_\upsilon \right) - \boldsymbol{\sigma}^\top \boldsymbol{\Phi}_\upsilon^\top \boldsymbol{\xi}_\upsilon(\boldsymbol{x}) \\ &\leq -\lambda_{\min}(\boldsymbol{Q}_m) \|\boldsymbol{e}\|^2 + \boldsymbol{\sigma}^\top \boldsymbol{G}(\boldsymbol{x}) \boldsymbol{u}_{s,\upsilon} \\ &\quad + \big(d_f^* + d_g^* \|\boldsymbol{u}_{a,\upsilon}\| + d_o \big) \|\boldsymbol{\sigma}\| \\ &\quad + \frac{1}{\kappa} \operatorname{trace}\left(\boldsymbol{\Phi}_\upsilon^\top \big(\dot{\boldsymbol{W}}_\upsilon - \kappa \boldsymbol{\xi}_\upsilon(\boldsymbol{x}) \boldsymbol{\sigma}^\top \big) \right) \\ &\leq -\lambda_{\min}(\boldsymbol{Q}_m) \|\boldsymbol{e}\|^2 + k_{s,\upsilon}^* \|\boldsymbol{\sigma}\| + \boldsymbol{\sigma}^\top \boldsymbol{G}(\boldsymbol{x}) \boldsymbol{u}_{s,\upsilon} \end{aligned} \tag{20}$$

where $k_{s,\upsilon}^* = d_f^* + d_g^* \|\boldsymbol{u}_{a,\upsilon}\| + d_o \leq k_{s,\upsilon}$. To proceed, two cases have to be analyzed. First, if $\|\boldsymbol{\sigma}\| > \nu$, then

$$k_{s,\upsilon}^* \|\boldsymbol{\sigma}\| + \boldsymbol{\sigma}^\top \boldsymbol{G}(\boldsymbol{x}) \boldsymbol{u}_{s,\upsilon} \leq k_{s,\upsilon}^* \|\boldsymbol{\sigma}\| - k_{s,\upsilon} \|\boldsymbol{\sigma}\| \leq 0. \tag{21}$$

If, on the other hand, $\|\boldsymbol{\sigma}\| \leq \nu$, then

$$\begin{aligned} k_{s,\upsilon}^* \|\boldsymbol{\sigma}\| + \boldsymbol{\sigma}^\top \boldsymbol{G}(\boldsymbol{x}) \boldsymbol{u}_{s,\upsilon} &\leq k_{s,\upsilon}^* \|\boldsymbol{\sigma}\| - k_{s,\upsilon}^* \frac{\|\boldsymbol{\sigma}\|^2}{\nu} \\ &= -k_{s,\upsilon}^* \left(\frac{\|\boldsymbol{\sigma}\|}{\sqrt{\nu}} - \frac{\sqrt{\nu}}{2} \right)^2 + \frac{k_{s,\upsilon}^*}{4} \nu \\ &\leq \frac{k_{s,\upsilon}^*}{4} \nu. \end{aligned} \tag{22}$$

Recall that $k_{s,\upsilon}^* = d_f^* + d_g^* \|\boldsymbol{u}_{a,\upsilon}\| + d_o$. Let

$$k_s^* = d_f^* + d_g^* \max_{\upsilon} \left(\max \|\boldsymbol{u}_{a,\upsilon}\| \right) + d_o \tag{23}$$

where the inner maximization is taken over $\boldsymbol{e} \in \boldsymbol{\Omega}_e$, $\boldsymbol{x}_d \in \boldsymbol{\Omega}_{x_d}$, $\boldsymbol{y}_d^{(n)} \in \boldsymbol{\Omega}_{y_d}$, and $\boldsymbol{\omega}_{i,\upsilon} \in \boldsymbol{\Omega}_{i,\upsilon}$. Combining (21) and (22), it gives

$$k_{s,\upsilon}^* \|\boldsymbol{\sigma}\| + \boldsymbol{\sigma}^\top \boldsymbol{G}(\boldsymbol{x}) \boldsymbol{u}_{s,\upsilon} \leq \frac{k_{s,\upsilon}^*}{4} \nu \leq \frac{k_s^*}{4} \nu. \tag{24}$$

It follows from (14) that

$$\frac{1}{2\kappa} \operatorname{trace}\left(\boldsymbol{\Phi}_\upsilon^\top \boldsymbol{\Phi}_\upsilon \right) = \sum_{i=1}^{p} \frac{1}{2\kappa} \boldsymbol{\phi}_{i,\upsilon}^\top \boldsymbol{\phi}_{i,\upsilon} \leq \sum_{i=1}^{p} c_i. \tag{25}$$

Let $\mu_m = \lambda_{\min}(\boldsymbol{Q}_m)/\lambda_{\max}(\boldsymbol{P}_m)$ and $c = \sum_{i=1}^{p} c_i$. Substituting (24) into (20) and taking into account (25) gives

$$\begin{aligned} \dot{V}_\upsilon &\leq -\lambda_{\min}(\boldsymbol{Q}_m) \|\boldsymbol{e}\|^2 + \frac{k_s^*}{4} \nu \\ &\leq -2\mu_m \frac{1}{2} \boldsymbol{e}^\top \boldsymbol{P}_m \boldsymbol{e} + \frac{k_s^*}{4} \nu \\ &\leq -2\mu_m V_\upsilon + 2\mu_m c + \frac{k_s^*}{4} \nu \\ &\leq -\mu_m V_\upsilon - \mu_m (V_\upsilon - 2\bar{c}) \end{aligned} \tag{26}$$

where $\bar{c} = c + (k_s^* \nu)/(8\mu_m)$. Let $t_{0,\upsilon}$ and $t_{f,\upsilon}$ denote the initial and the final time, respectively, of the period during which the controller is in the υth mode. It follows from (26) that if $V_\upsilon(t) \geq 2\bar{c}$ for $t \in [t_{0,\upsilon}, t_{f,\upsilon}]$, then $\dot{V}_\upsilon(t) \leq -\mu_m V_\upsilon(t)$, which implies that

$$V_\upsilon(t) \leq \exp(-\mu_m (t - t_{0,\upsilon})) V_\upsilon(t_{0,\upsilon}) \tag{27}$$

for $t \in [t_{0,\upsilon}, t_{f,\upsilon}]$.

Theorem 1: Let t_1, t_2, and t_3 be three consecutive switching time instants so that $\upsilon = \upsilon_1$ for $t \in [t_1, t_2)$ and $\upsilon = \upsilon_2$ for $t \in [t_2, t_3)$. Suppose that $V_\upsilon(t) \geq 2\bar{c}$ for $t \in [t_1, t_3)$. If one of the following two mutually exclusive conditions are satisfied, then $V_{\upsilon_2}(t_2) < V_{\upsilon_1}(t_1)$ and $V_{\upsilon_2}(t_3^-) < V_{\upsilon_1}(t_2^-)$.

1) The dwell time T_d of the variable-structure RBF network is selected such that
$$T_d \geq \frac{1}{\mu_m} \ln\left(\frac{3}{2}\right). \tag{28}$$
2) The constants c and ν satisfy the following inequality when T_d does not satisfy (28),
$$0 < c < \frac{\exp(\mu_m T_d) - 1}{3 - 2\exp(\mu_m T_d)} \frac{k_s^* \nu}{4\mu_m}. \tag{29}$$

Proof: When the controller switches from the υ_1th to the υ_2th mode, there exists a jump between $V_{\upsilon_2}(t_2)$ and $V_{\upsilon_1}(t_2^-)$, which is denoted as
$$\Delta = V_{\upsilon_2}(t_2) - V_{\upsilon_1}(t_2^-). \tag{30}$$
Because $\boldsymbol{x}$ and $\boldsymbol{x}_d$ are continuous, therefore $\boldsymbol{e}$ is continuous. Hence, it follows from (19) and (25) that
$$\begin{aligned}\Delta = &\frac{1}{2\kappa} \operatorname{trace}\left(\boldsymbol{\Phi}_{\upsilon_2}^\top(t_2)\boldsymbol{\Phi}_{\upsilon_2}(t_2)\right) \\ &-\frac{1}{2\kappa} \operatorname{trace}\left(\boldsymbol{\Phi}_{\upsilon_1}^\top(t_2^-)\boldsymbol{\Phi}_{\upsilon_1}(t_2^-)\right)\end{aligned}$$
and $|\Delta| \leq c$. Because $V_{\upsilon_2}(t) \geq 2\bar{c}$ for $t \in [t_2, t_3)$, it follows from (27) and (30) that
$$\begin{aligned}V_{\upsilon_2}(t_3^-) &\leq \exp(-\mu_m(t_3 - t_2))V_{\upsilon_2}(t_2) \\ &= \exp(-\mu_m(t_3 - t_2))\left(V_{\upsilon_1}(t_2^-) + \Delta\right) \\ &\leq \exp(-\mu_m(t_3 - t_2))\left(V_{\upsilon_1}(t_2^-) + c\right).\end{aligned}$$
Due to the dwell time requirement on the variable-structure RBF network, it is true that $t_3 - t_2 \geq T_d$, which implies that $\exp(-\mu_m(t_3 - t_2)) \leq \exp(-\mu_m T_d)$. Therefore, $V_{\upsilon_2}(t_3^-) \leq \exp(-\mu_m T_d)\left(V_{\upsilon_1}(t_2^-) + c\right)$. To obtain $V_{\upsilon_2}(t_3^-) < V_{\upsilon_1}(t_2^-)$, it is sufficient that
$$\exp(-\mu_m T_d)\left(V_{\upsilon_1}(t_2^-) + c\right) < V_{\upsilon_1}(t_2^-). \tag{31}$$
Now, two different cases are analyzed.

Case (a): For fixed c and ν, solve (31) for T_d to obtain
$$T_d > \frac{1}{\mu_m} \ln\left(\frac{V_{\upsilon_1}(t_2^-) + c}{V_{\upsilon_1}(t_2^-)}\right).$$
It is easy to verify that the right-hand side of the above inequality is a decreasing function of $V_{\upsilon_1}(t_2^-)$ when $V_{\upsilon_1}(t_2^-) \geq 2\bar{c}$. Recall that $\bar{c} = c + k_s^*\nu/(8\mu_m) > c$. It follows that
$$\ln\left(\frac{V_{\upsilon_1}(t_2^-) + c}{V_{\upsilon_1}(t_2^-)}\right) \leq \ln\left(\frac{2\bar{c} + c}{2\bar{c}}\right) < \ln\left(\frac{3}{2}\right).$$
Therefore, if T_d satisfies (28), then (31) is satisfied, which implies that $V_{\upsilon_2}(t_3^-) < V_{\upsilon_1}(t_2^-)$.

Case (b): For each fixed T_d, solve (31) for c to obtain $c < (\exp(\mu_m T_d) - 1)\, V_{\upsilon_1}(t_2^-)$. Note that $V_{\upsilon_1}(t_2^-) \geq 2\bar{c}$ and $\bar{c} = c + k_s^*\nu/(8\mu_m)$. To guarantee the above, it is enough that
$$c < 2\left(\exp(\mu_m T_d) - 1\right)\left(c + \frac{k_s^*\nu}{8\mu_m}\right). \tag{32}$$
If T_d does not satisfy (28), that is, $0 < T_d < \ln(3/2)/\mu_m$, it is easy to verify that $2\exp(\mu_m T_d) < 3$. Then, solving (32) for c, it gives
$$0 < c < \frac{\exp(\mu_m T_d) - 1}{3 - 2\exp(\mu_m T_d)} \frac{k_s^*\nu}{4\mu_m}$$
which guarantees (31) and then $V_{\upsilon_2}(t_3^-) < V_{\upsilon_1}(t_2^-)$.

On the other hand, because $V_{\upsilon_1}(t) \geq 2\bar{c}$ for $t \in [t_1, t_2)$, it follows from (27) that $V_{\upsilon_1}(t_2^-) \leq \exp(-\mu_m(t_2 - t_1))V_{\upsilon_1}(t_1)$, which implies that
$$V_{\upsilon_1}(t_1) \geq \exp(\mu_m(t_2 - t_1))V_{\upsilon_1}(t_2^-) \geq \exp(\mu_m T_d)V_{\upsilon_1}(t_2^-)$$
as $t_2 - t_1 \geq T_d$. Note that, for both conditions given by (28) and (29), $V_{\upsilon_1}(t_2^-) > \exp(-\mu_m T_d)\left(V_{\upsilon_1}(t_2^-) + c\right)$. Then, it follows that
$$V_{\upsilon_1}(t_1) \geq \exp(\mu_m T_d)V_{\upsilon_1}(t_2^-) > V_{\upsilon_1}(t_2^-) + c \geq V_{\upsilon_2}(t_2)$$
where $V_{\upsilon_2}(t_2) = V_{\upsilon_1}(t_2^-) + \Delta$.

In summary, if either one of the conditions (28) or (29) is satisfied, then $V_{\upsilon_2}(t_2) < V_{\upsilon_1}(t_1)$ and $V_{\upsilon_2}(t_3^-) < V_{\upsilon_1}(t_2^-)$. ■

Remark 6: Recall that $c = \sum_{i=1}^p c_i$. It follows from (14) that one can decrease c_i, and thus c, by increasing κ. Hence, (29) can always be satisfied by selecting a large κ. However, this may lead to excessively large values of κ, which can adversely impact the adaptation law (15). Thus, choosing the dwell time T_d to satisfy condition (a) is typically the one that can be practically used. Condition (b) is included in Theorem 1 only for theoretical completeness to show that the system stability may still be guaranteed even when condition (a) fails, i.e., with a small T_d.

The following corollary easily follows from Theorem 1.

Corollary 1: If one of the conditions (28) or (29) is satisfied, then $V_\upsilon(t)$ will visit the interval $[0, 2\bar{c}]$ infinitely often. That is, for any $T \geq t_0$, there exists a time $t \geq T$ such that $V_\upsilon(t) \leq 2\bar{c}$.

Theorem 2: For the system (2) driven by the adaptive robust state feedback controller (12) with the robustifying component (18) and the adaptation law (15), suppose that one of the conditions (28) or (29) is satisfied. If $c_e \geq \max\left\{c_{e_0} + c, 2\bar{c} + c\right\}$, then $\boldsymbol{e}(t) \in \boldsymbol{\Omega}_e$ and $\boldsymbol{x}(t) \in \boldsymbol{\Omega}_x$ for $t \geq t_0$. Moreover, there exists a finite time $T \geq t_0$ such that
$$\frac{1}{2}\boldsymbol{e}^\top(t)\boldsymbol{P}_m\boldsymbol{e}(t) \leq 2\bar{c} + c \tag{33}$$
for $t \geq T$.

Proof: If T_d satisfies (28) or, otherwise, the constants c and ν satisfy (29), it follows from Corollary 1 that $V_\upsilon(t)$ will visit the interval $[0, 2\bar{c}]$ infinitely often. Let $T \geq t_0$ be the first time instant such that $V_\upsilon(T) \leq 2\bar{c}$. The trajectory of $V_\upsilon(t)$ starting at $t = T$ will stay inside the interval $[0, 2\bar{c}]$ until it jumps outside when the controller switches its mode. However, the jump of $V_\upsilon(t)$ between different modes satisfies that $|\Delta| \leq c$. Hence, $V_\upsilon(t) \leq 2\bar{c} + c$ for $t \geq T$.

On the other hand, it is known that $V_\upsilon(t_0) \leq c_{e_0} + c$. If $c_e \geq \max\left\{c_{e_0} + c, 2\bar{c} + c\right\}$, then $V_\upsilon(t) \leq c_e$ for $t \geq t_0$. It follows from $\frac{1}{2}\boldsymbol{e}^\top(t)\boldsymbol{P}_m\boldsymbol{e}(t) \leq V_\upsilon(t)$ that $\frac{1}{2}\boldsymbol{e}^\top(t)\boldsymbol{P}_m\boldsymbol{e}(t) \leq c_e$, which implies that $\boldsymbol{e}(t) \in \boldsymbol{\Omega}_e$ and $\boldsymbol{x}(t) \in \boldsymbol{\Omega}_x$, for $t \geq t_0$. Moreover, $\frac{1}{2}\boldsymbol{e}^\top(t)\boldsymbol{P}_m\boldsymbol{e}(t) \leq 2\bar{c} + c$ for $t \geq T$. ■

Note that, in the above theorem, the controller could keep switching between different modes all the time. The following result is concerned with a special case when the switching of the controller mode stops after a finite time.

Corollary 2: Suppose that either T_d satisfies (28) or the constants c and ν satisfy (29). In addition, suppose that there exists a finite time $T_s \geq t_0$ such that $\upsilon = \upsilon_s$ for $t \geq T_s$. If $c_e \geq \max\{c_{e_0} + c, 2\bar{c} + c\}$, then $\boldsymbol{e}(t) \in \boldsymbol{\Omega}_e$ and $\boldsymbol{x}(t) \in \boldsymbol{\Omega}_x$ for $t \geq t_0$, and there exists a finite time $T \geq T_s$ such that

$$\frac{1}{2}\boldsymbol{e}^\top(t)\boldsymbol{P}_m\boldsymbol{e}(t) \leq 2\bar{c} \tag{34}$$

for $t \geq T$.

Proof: If either T_d satisfies (28) or the constants c and ν satisfy (29), it follows from Theorem 2 that if $c_e \geq \max\{c_{e_0} + c, 2\bar{c} + c\}$, then $\boldsymbol{e}(t) \in \boldsymbol{\Omega}_e$ and $\boldsymbol{x}(t) \in \boldsymbol{\Omega}_x$ for $t \geq t_0$. If, in addition, $\upsilon = \upsilon_s$ for $t \geq T_s$, then it follows from (26) that $\dot{V}_{\upsilon_s} \leq -\mu_m V_{\upsilon_s} - \mu_m(V_{\upsilon_s} - 2\bar{c})$ for $t \geq T_s$. Thus, there exists a finite time $T \geq T_s$ such that $V_{\upsilon_s} \leq 2\bar{c}$, which implies that $\frac{1}{2}\boldsymbol{e}^\top(t)\boldsymbol{P}_m\boldsymbol{e}(t) \leq 2\bar{c}$, for $t \geq T$. ∎

Remark 7: It can be seen from (33) and (34) that the tracking performance is directly proportional to the magnitude of c and ν. Recall that the magnitude of c is inversely proportional to κ. Therefore, increasing κ and decreasing ν would result in better tracking performance.

V. Output Feedback Controller Construction

In the development of the adaptive robust state feedback in the previous section, the availability of the system states has been assumed. However, in practical applications, often only the system outputs are available. Thus, it is desirable to develop an adaptive robust output feedback controller. In the following, it is assumed that the system output measurements are of high accuracy. The measurement noise will have a detrimental effect on the performance of the proposed output feedback controller. This is because not only will the adaptive component fit to the measurement noise but also the output tracking accuracy cannot be guaranteed.

A. High-Gain Tracking Error Observer

Let $\hat{e}_{yi}$ be the estimate of the ith output tracking error and let $\hat{\boldsymbol{e}}_i = [\hat{e}_{yi} \ \cdots \ \hat{e}_{yi}^{(n_i-1)}]^\top$. To proceed, apply the following high-gain observer [8], [14],

$$\dot{\hat{\boldsymbol{e}}}_i = \boldsymbol{A}_i\hat{\boldsymbol{e}}_i + \boldsymbol{l}_i\left(e_{yi} - \boldsymbol{c}_i\hat{\boldsymbol{e}}_i\right), \qquad i = 1, \ldots, p \tag{35}$$

to estimate the tracking error of the ith subsystem $\boldsymbol{e}_i$. The observer gain $\boldsymbol{l}_i$ is chosen as $\boldsymbol{l}_i = [\alpha_{i1}/\epsilon \ \cdots \ \alpha_{in_i}/\epsilon^{n_i}]^\top$, where $\epsilon \in (0, 1)$ is a design parameter and α_{ij}, $j = 1, \ldots, n_i$, are selected so that the roots of the characteristic polynomial equation, $s^{n_i} + \alpha_{i1}s^{n_i-1} + \cdots + \alpha_{i(n_i-1)}s + \alpha_{in_i} = 0$, have negative real parts. Let $\hat{\boldsymbol{e}} = [\hat{\boldsymbol{e}}_1^\top \ \cdots \ \hat{\boldsymbol{e}}_p^\top]^\top$ and let $\boldsymbol{L} = \text{diag}[\boldsymbol{l}_1 \ \cdots \ \boldsymbol{l}_p]$. Then, the high-gain observer (35) can be represented in a compact form as

$$\dot{\hat{\boldsymbol{e}}} = \boldsymbol{A}\hat{\boldsymbol{e}} + \boldsymbol{L}\big(\boldsymbol{e}_y - \boldsymbol{C}\hat{\boldsymbol{e}}\big). \tag{36}$$

To facilitate the stability analysis of the closed-loop system, the dynamics of the estimation error are represented in the singularly perturbed form. Let $\boldsymbol{\zeta} = [\boldsymbol{\zeta}_1^\top \ \cdots \ \boldsymbol{\zeta}_p^\top]^\top$, where $\boldsymbol{\zeta}_i = [\zeta_{i1} \ \cdots \ \zeta_{in_i}]^\top$ with

$$\zeta_{ij} = \frac{e_{yi}^{(j-1)} - \hat{e}_{yi}^{(j-1)}}{\epsilon^{n_i-j}}, \quad j = 1, \ldots, n_i. \tag{37}$$

It follows from (37) that $\hat{\boldsymbol{e}} = \boldsymbol{e} - \boldsymbol{D}\boldsymbol{\zeta}$, where $\boldsymbol{D} = \text{diag}[\boldsymbol{D}_1 \ \cdots \ \boldsymbol{D}_p]$ and $\boldsymbol{D}_i = \text{diag}[\epsilon^{n_i-1} \ \cdots \ 1]$. Note that $\|\boldsymbol{D}\| = 1$. Taking into account (4) and (36) yields

$$\epsilon\dot{\boldsymbol{\zeta}} = \boldsymbol{A}_c\boldsymbol{\zeta} + \epsilon\boldsymbol{B}\big(\boldsymbol{f}(\boldsymbol{x}) + \boldsymbol{G}(\boldsymbol{x})\boldsymbol{u} - \boldsymbol{y}_d^{(n)} + \boldsymbol{d}\big) \tag{38}$$

where $\boldsymbol{A}_c = \text{diag}[\boldsymbol{A}_{c1} \ \cdots \ \boldsymbol{A}_{cp}]$ and $\boldsymbol{A}_{ci} = \epsilon\boldsymbol{D}_i^{-1}(\boldsymbol{A}_i - \boldsymbol{l}_i\boldsymbol{c}_i)\boldsymbol{D}_i$ is a Hurwitz matrix. Applying the method from [30] and [31], the following proposition can be proved.

Proposition 1: Suppose that the controller $\boldsymbol{u}$ in (38) is globally bounded. Then, there exists a constant $\epsilon_1^* \in (0, 1)$ such that if $\epsilon \in (0, \epsilon_1^*)$, then $\|\boldsymbol{\zeta}(t)\| \leq \beta\epsilon$ with some $\beta > 0$ for $t \in [t_0 + T_1(\epsilon), t_0 + T_3)$, where $T_1(\epsilon)$ is a finite time and $t_0 + T_3$ is the moment when the tracking error $\boldsymbol{e}(t)$ leaves the compact set $\boldsymbol{\Omega}_e$ for the first time. Moreover, $\lim_{\epsilon\to 0^+} T_1(\epsilon) = 0$ and $c_{e_1} = \frac{1}{2}\boldsymbol{e}(t_0 + T_1(\epsilon))^\top\boldsymbol{P}_m\boldsymbol{e}(t_0 + T_1(\epsilon)) < c_e$.

B. Controller Design

Let $\hat{\boldsymbol{x}} = \boldsymbol{x}_d + \hat{\boldsymbol{e}}$. Substituting $\hat{\boldsymbol{x}}$ and $\hat{\boldsymbol{e}}$ for $\boldsymbol{x}$ and $\boldsymbol{e}$, respectively, into the controller $\boldsymbol{u}$ in (12) with (18) yields

$$\hat{\boldsymbol{u}} = \hat{\boldsymbol{u}}_{a,\upsilon} + \hat{\boldsymbol{u}}_{s,\upsilon} \tag{39}$$

with $\hat{\boldsymbol{u}}_{a,\upsilon} = \boldsymbol{G}_0^{-1}(-\hat{\boldsymbol{f}}_\upsilon(\hat{\boldsymbol{x}}) + \boldsymbol{y}_d^{(n)} - \boldsymbol{K}\hat{\boldsymbol{e}})$ and

$$\hat{\boldsymbol{u}}_{s,\upsilon} = \begin{cases} -\dfrac{\hat{k}_{s,\upsilon}}{\underline{g}}\dfrac{\hat{\boldsymbol{\sigma}}}{\|\hat{\boldsymbol{\sigma}}\|} & \text{if } \|\hat{\boldsymbol{\sigma}}\| \geq \nu \\ -\dfrac{\hat{k}_{s,\upsilon}}{\underline{g}}\dfrac{\hat{\boldsymbol{\sigma}}}{\mu} & \text{if } \|\hat{\boldsymbol{\sigma}}\| < \nu \end{cases}$$

where $\hat{k}_{s,\upsilon} = d_f + d_g\|\hat{\boldsymbol{u}}_{a,\upsilon}\| + d_o$ and $\hat{\boldsymbol{\sigma}} = \boldsymbol{B}^\top\boldsymbol{P}_m\hat{\boldsymbol{e}}$. Accordingly, the adaptation for the weight matrix $\boldsymbol{W}_\upsilon$ takes the form

$$\dot{\boldsymbol{W}}_\upsilon = \text{Proj}\left(\boldsymbol{W}_\upsilon, \kappa\boldsymbol{\xi}_\upsilon(\hat{\boldsymbol{x}})\hat{\boldsymbol{\sigma}}^\top\right) \tag{40}$$

which ensures that

$$\frac{1}{\kappa}\,\text{trace}\left(\boldsymbol{\Phi}_\upsilon^\top\left(\dot{\boldsymbol{W}}_\upsilon - \kappa\boldsymbol{\xi}_\upsilon(\hat{\boldsymbol{x}})\hat{\boldsymbol{\sigma}}^\top\right)\right) \leq 0. \tag{41}$$

Recall that associated with the high-gain observer described by (36), there exist peaking phenomena [31], [32]. This prevents us from directly applying the controller (39) obtained by replacing $\boldsymbol{e}$ with $\hat{\boldsymbol{e}}$ in the state feedback controller (12). To eliminate the peaking phenomena, saturation on the control input (39) is introduced as in [31]. Let $\boldsymbol{\Omega}_{\hat{e}} = \{\boldsymbol{e} : \frac{1}{2}\boldsymbol{e}^\top\boldsymbol{P}_m\boldsymbol{e} \leq c_{\hat{e}}\}$, where $c_{\hat{e}} > c_e$, and let

$$U_i \geq \max_\upsilon\left(\max\left|u_i\left(\boldsymbol{e}, \boldsymbol{x}_d, \boldsymbol{y}_{di}^{(n)}, \boldsymbol{\omega}_{i,\upsilon}\right)\right|\right)$$

where u_i is the ith element of $\boldsymbol{u}$ defined in (12), and the inner maximization is taken over $\boldsymbol{e} \in \boldsymbol{\Omega}_{\hat{e}}$, $\boldsymbol{x}_d \in \boldsymbol{\Omega}_{x_d}$, $\boldsymbol{y}_{di}^{(n)} \in \boldsymbol{\Omega}_{y_{di}}$, and $\boldsymbol{\omega}_{i,\upsilon} \in \boldsymbol{\Omega}_{i,\upsilon}$. Then, the proposed adaptive robust output feedback controller takes the form

$$\boldsymbol{u}^s = \left[U_1\,\text{sat}\left(\frac{\hat{u}_1}{U_1}\right) \ \cdots \ U_p\,\text{sat}\left(\frac{\hat{u}_p}{U_p}\right)\right]^\top \tag{42}$$

where sat is the saturation function defined as

$$\text{sat}\left(\frac{\hat{u}_i}{U_i}\right) = \max\left\{\min\left\{\frac{\hat{u}_i}{U_i}, 1\right\}, -1\right\}.$$

Note that the control input is globally bounded by construction. Hence, it follows from Proposition 1 that if $\epsilon \in (0, \epsilon_1^*)$, then $\boldsymbol{e}(t) \in \boldsymbol{\Omega}_e$ and $\|\boldsymbol{\zeta}(t)\| \le \beta\epsilon$ for $t \in [t_0 + T_1(\epsilon), t_0 + T_3)$. Thus, $\|\boldsymbol{e}(t) - \hat{\boldsymbol{e}}(t)\| \le \|\boldsymbol{D}\|\|\boldsymbol{\zeta}(t)\| \le \beta\epsilon$ for $t \in [t_0 + T_1(\epsilon), t_0 + T_3)$. There exists a constant ϵ_2 such that if $\|\boldsymbol{e}(t) - \hat{\boldsymbol{e}}(t)\| \le \beta\epsilon_2$, then $\hat{\boldsymbol{e}}(t) \in \boldsymbol{\Omega}_{\hat{e}}$. Let $\epsilon_2^* = \min\{\epsilon_1^*, \epsilon_2\}$. If $\epsilon \in (0, \epsilon_2^*)$, the saturation of the adaptive robust output feedback (42) is not effective, that is, $\boldsymbol{u}^s = \hat{\boldsymbol{u}} = \hat{\boldsymbol{u}}_{a,\upsilon} + \hat{\boldsymbol{u}}_{s,\upsilon}$ for $t \in [t_0 + T_1(\epsilon), t_0 + T_3)$. Substituting $\boldsymbol{u}^s = \hat{\boldsymbol{u}}_{a,\upsilon} + \hat{\boldsymbol{u}}_{s,\upsilon}$ into (4) gives

$$\begin{aligned}
\dot{\boldsymbol{e}} &= \boldsymbol{A}\boldsymbol{e} + \boldsymbol{B}\big(\boldsymbol{f}(\boldsymbol{x}) + \boldsymbol{G}(\boldsymbol{x})\big(\hat{\boldsymbol{u}}_{a,\upsilon} + \hat{\boldsymbol{u}}_{s,\upsilon}\big) - \boldsymbol{y}_d^{(n)} + \boldsymbol{d}\big) \\
&= \boldsymbol{A}\boldsymbol{e} + \boldsymbol{B}\big(\hat{\boldsymbol{f}}_\upsilon(\hat{\boldsymbol{x}}) + \boldsymbol{G}_0\hat{\boldsymbol{u}}_{a,\upsilon} - \boldsymbol{y}_d^{(n)}\big) \\
&\quad + \boldsymbol{B}\big(\boldsymbol{f}(\boldsymbol{x}) - \hat{\boldsymbol{f}}_\upsilon(\hat{\boldsymbol{x}}) + \big(\boldsymbol{G}(\boldsymbol{x}) - \boldsymbol{G}_0\big)\hat{\boldsymbol{u}}_{a,\upsilon}\big) \\
&\quad + \boldsymbol{B}\big(+\boldsymbol{G}(\boldsymbol{x})\hat{\boldsymbol{u}}_{s,\upsilon} + \boldsymbol{d}\big) \\
&= \boldsymbol{A}_m\boldsymbol{e} + \boldsymbol{B}\boldsymbol{K}(\boldsymbol{e} - \hat{\boldsymbol{e}}) + \boldsymbol{B}\boldsymbol{G}(\boldsymbol{x})\hat{\boldsymbol{u}}_{s,\upsilon} \\
&\quad + \boldsymbol{B}\big(\boldsymbol{f}(\boldsymbol{x}) - \hat{\boldsymbol{f}}_\upsilon(\hat{\boldsymbol{x}}) + \big(\boldsymbol{G}(\boldsymbol{x}) - \boldsymbol{G}_0\big)\hat{\boldsymbol{u}}_{a,\upsilon} + \boldsymbol{d}\big). \qquad (43)
\end{aligned}$$

Now, consider the same piecewise quadratic Lyapunov function as in (19) for $t \in [t_0 + T_1(\epsilon), t_0 + T_3)$ and $\epsilon \in (0, \epsilon_2^*)$. The time derivative of V_υ evaluated on the solutions of (43) takes the following form,

$$\begin{aligned}
\dot{V}_\upsilon &= \boldsymbol{e}^\top\boldsymbol{P}_m\dot{\boldsymbol{e}} + \frac{1}{\kappa}\text{trace}\left(\boldsymbol{\Phi}_\upsilon^\top\dot{\boldsymbol{\Phi}}_\upsilon\right) \\
&= \boldsymbol{e}^\top\boldsymbol{P}_m\boldsymbol{A}_m\boldsymbol{e} + \boldsymbol{\sigma}^\top\boldsymbol{K}(\boldsymbol{e} - \hat{\boldsymbol{e}}) \\
&\quad + \boldsymbol{\sigma}^\top\boldsymbol{G}(\boldsymbol{x})\hat{\boldsymbol{u}}_{s,\upsilon} + \frac{1}{\kappa}\text{trace}\left(\boldsymbol{\Phi}_\upsilon^\top\dot{\boldsymbol{\Phi}}_\upsilon\right) \\
&\quad + \boldsymbol{\sigma}^\top\big(\boldsymbol{f}(\boldsymbol{x}) - \hat{\boldsymbol{f}}_\upsilon(\hat{\boldsymbol{x}}) + \big(\boldsymbol{G}(\boldsymbol{x}) - \boldsymbol{G}_0\big)\hat{\boldsymbol{u}}_{a,\upsilon} + \boldsymbol{d}\big) \\
&= -\boldsymbol{e}^\top\boldsymbol{Q}_m\boldsymbol{e} + \boldsymbol{\sigma}^\top\boldsymbol{K}(\boldsymbol{e} - \hat{\boldsymbol{e}}) \\
&\quad + \hat{\boldsymbol{\sigma}}^\top\boldsymbol{G}(\boldsymbol{x})\hat{\boldsymbol{u}}_{s,\upsilon} + \frac{1}{\kappa}\text{trace}\left(\boldsymbol{\Phi}_\upsilon^\top\dot{\boldsymbol{\Phi}}_\upsilon\right) \\
&\quad + \hat{\boldsymbol{\sigma}}^\top\big(\boldsymbol{f}(\boldsymbol{x}) - \hat{\boldsymbol{f}}_\upsilon(\hat{\boldsymbol{x}}) + \big(\boldsymbol{G}(\boldsymbol{x}) - \boldsymbol{G}_0\big)\hat{\boldsymbol{u}}_{a,\upsilon} + \boldsymbol{d}\big) \\
&\quad + \big(\boldsymbol{\sigma} - \hat{\boldsymbol{\sigma}}\big)^\top\big(\boldsymbol{f}(\boldsymbol{x}) - \hat{\boldsymbol{f}}_\upsilon(\hat{\boldsymbol{x}}) + \big(\boldsymbol{G}(\boldsymbol{x}) - \boldsymbol{G}_0\big)\hat{\boldsymbol{u}}_{a,\upsilon}\big) \\
&\quad + \big(\boldsymbol{\sigma} - \hat{\boldsymbol{\sigma}}\big)^\top\big(\boldsymbol{d} + \boldsymbol{G}(\boldsymbol{x})\hat{\boldsymbol{u}}_{s,\upsilon}\big) \\
&= -\boldsymbol{e}^\top\boldsymbol{Q}_m\boldsymbol{e} + \boldsymbol{\sigma}^\top\boldsymbol{K}(\boldsymbol{e} - \hat{\boldsymbol{e}}) + \hat{\boldsymbol{\sigma}}^\top\boldsymbol{G}(\boldsymbol{x})\hat{\boldsymbol{u}}_{s,\upsilon} \\
&\quad + \frac{1}{\kappa}\text{trace}\left(\boldsymbol{\Phi}_\upsilon^\top\big(\dot{\boldsymbol{W}}_\upsilon - \kappa\boldsymbol{\xi}_\upsilon(\hat{\boldsymbol{x}})\hat{\boldsymbol{\sigma}}^\top\big)\right) + \hat{\boldsymbol{\sigma}}^\top\boldsymbol{d} \\
&\quad + \hat{\boldsymbol{\sigma}}^\top\big(\boldsymbol{f}(\boldsymbol{x}) - \boldsymbol{W}_\upsilon^{*\top}\boldsymbol{\xi}_\upsilon(\hat{\boldsymbol{x}})\big) + \hat{\boldsymbol{\sigma}}^\top\big(\boldsymbol{G}(\boldsymbol{x}) - \boldsymbol{G}_0\big)\hat{\boldsymbol{u}}_{a,\upsilon} \\
&\quad + \big(\boldsymbol{\sigma} - \hat{\boldsymbol{\sigma}}\big)^\top\big(\boldsymbol{f}(\boldsymbol{x}) - \hat{\boldsymbol{f}}_\upsilon(\hat{\boldsymbol{x}}) + \big(\boldsymbol{G}(\boldsymbol{x}) - \boldsymbol{G}_0\big)\hat{\boldsymbol{u}}_{a,\upsilon}\big) \\
&\quad + \big(\boldsymbol{\sigma} - \hat{\boldsymbol{\sigma}}\big)^\top\big(\boldsymbol{d} + \boldsymbol{G}(\boldsymbol{x})\hat{\boldsymbol{u}}_{s,\upsilon}\big). \qquad (44)
\end{aligned}$$

For $t \in [t_0 + T_1(\epsilon), t_0 + T_3)$, if $\epsilon \in (0, \epsilon_2^*)$, $\|\boldsymbol{\zeta}(t)\| \le \beta\epsilon$, $\|\boldsymbol{e}(t) - \hat{\boldsymbol{e}}(t)\| \le \beta\epsilon$, $\boldsymbol{e}(t) \in \boldsymbol{\Omega}_e$, $\hat{\boldsymbol{e}}(t) \in \boldsymbol{\Omega}_{\hat{e}}$, $\boldsymbol{x}_d(t) \in \boldsymbol{\Omega}_{x_d}$, and $\boldsymbol{y}_d^{(n)}(t) \in \boldsymbol{\Omega}_{y_d}$. Hence, $\boldsymbol{\sigma}(t)$, $\hat{\boldsymbol{\sigma}}(t)$, $\boldsymbol{x}(t)$, $\hat{\boldsymbol{x}}(t)$, $\hat{\boldsymbol{u}}_{a,\upsilon}(t)$, and $\hat{\boldsymbol{u}}_{s,\upsilon}(t)$ are all bounded for $t \in [t_0 + T_1(\epsilon), t_0 + T_3)$. Thus

$$\left\|\boldsymbol{\sigma}^\top\boldsymbol{K}(\boldsymbol{e} - \hat{\boldsymbol{e}})\right\| \le r_1\epsilon \qquad (45)$$

and

$$\left\|\begin{aligned}\big(\boldsymbol{\sigma} - \hat{\boldsymbol{\sigma}}\big)^\top\Big(\boldsymbol{f}(\boldsymbol{x}) - \hat{\boldsymbol{f}}_\upsilon(\hat{\boldsymbol{x}}) + \big(\boldsymbol{G}(\boldsymbol{x}) - \boldsymbol{G}_0\big)\hat{\boldsymbol{u}}_{a,\upsilon}\Big) \\ + \big(\boldsymbol{\sigma} - \hat{\boldsymbol{\sigma}}\big)^\top\big(\boldsymbol{d} + \boldsymbol{G}(\boldsymbol{x})\hat{\boldsymbol{u}}_{s,\upsilon}\big)\end{aligned}\right\| \le r_2\epsilon \qquad (46)$$

for some $r_1, r_2 > 0$. On the other hand, it follows from the Lipschitz continuity of the RCRBF that

$$\left\|\boldsymbol{W}_\upsilon^{*\top}\boldsymbol{\xi}_\upsilon(\boldsymbol{x}) - \boldsymbol{W}_\upsilon^{*\top}\boldsymbol{\xi}_\upsilon(\hat{\boldsymbol{x}})\right\| \le L_\upsilon\|\boldsymbol{x} - \hat{\boldsymbol{x}}\|$$

for some $L_\upsilon > 0$. Let $L = \max_\upsilon L_\upsilon$. Taking into account that $\|\boldsymbol{x} - \hat{\boldsymbol{x}}\| = \|\boldsymbol{e} - \hat{\boldsymbol{e}}\|$, it gives

$$\begin{aligned}
&\left\|\hat{\boldsymbol{\sigma}}^\top\big(\boldsymbol{f}(\boldsymbol{x}) - \boldsymbol{W}_\upsilon^{*\top}\boldsymbol{\xi}_\upsilon(\hat{\boldsymbol{x}})\big)\right\| \\
&\qquad \le \left\|\boldsymbol{f}(\boldsymbol{x}) - \boldsymbol{W}_\upsilon^{*\top}\boldsymbol{\xi}_\upsilon(\boldsymbol{x})\right\|\|\hat{\boldsymbol{\sigma}}\| \\
&\qquad\quad + \left\|\boldsymbol{W}_\upsilon^{*\top}\boldsymbol{\xi}_\upsilon(\boldsymbol{x}) - \boldsymbol{W}_\upsilon^{*\top}\boldsymbol{\xi}_\upsilon(\hat{\boldsymbol{x}})\right\|\|\hat{\boldsymbol{\sigma}}\| \\
&\qquad \le d_f^*\|\hat{\boldsymbol{\sigma}}\| + L\|\boldsymbol{e} - \hat{\boldsymbol{e}}\|\|\hat{\boldsymbol{\sigma}}\| \\
&\qquad \le d_f^*\|\hat{\boldsymbol{\sigma}}\| + r_3\epsilon \qquad (47)
\end{aligned}$$

for some $r_3 > 0$. It follows from (41) and (44)–(47) that

$$\begin{aligned}
\dot{V}_\upsilon &\le -\boldsymbol{e}^\top\boldsymbol{Q}_m\boldsymbol{e} + \big(d_f^* + d_g^*\|\hat{\boldsymbol{u}}_{a,\upsilon}\| + d_o\big)\|\hat{\boldsymbol{\sigma}}\| \\
&\quad + \hat{\boldsymbol{\sigma}}^\top\boldsymbol{G}(\boldsymbol{x})\hat{\boldsymbol{u}}_{s,\upsilon} + (r_1 + r_2 + r_3)\epsilon \\
&\le -\boldsymbol{e}^\top\boldsymbol{Q}_m\boldsymbol{e} + \hat{k}_{s,\upsilon}^*\|\hat{\boldsymbol{\sigma}}\| + \hat{\boldsymbol{\sigma}}^\top\boldsymbol{G}(\boldsymbol{x})\hat{\boldsymbol{u}}_{s,\upsilon} + r\epsilon \qquad (48)
\end{aligned}$$

where $r = r_1 + r_2 + r_3$ and $\hat{k}_{s,\upsilon}^* = d_f^* + d_g^*\|\hat{\boldsymbol{u}}_{a,\upsilon}\| + d_o \le \hat{k}_{s,\upsilon}$. Applying the same arguments that are used to obtain (21) and (22) yields

$$\hat{k}_{s,\upsilon}^*\|\hat{\boldsymbol{\sigma}}\| + \hat{\boldsymbol{\sigma}}^\top\boldsymbol{G}(\boldsymbol{x})\hat{\boldsymbol{u}}_{s,\upsilon} \le \frac{\hat{k}_{s,\upsilon}^*}{4}\nu \le \frac{\hat{k}_s^*}{4}\nu \qquad (49)$$

with $\hat{k}_s^* = d_f^* + d_g^*\max_\upsilon\left(\max\|\hat{\boldsymbol{u}}_{a,\upsilon}\|\right) + d_o$, where the inner maximization is taken over $\boldsymbol{x}_d \in \boldsymbol{\Omega}_{x_d}$, $\boldsymbol{y}_d^{(n)} \in \boldsymbol{\Omega}_{y_d}$, and $\hat{\boldsymbol{e}} \in \boldsymbol{\Omega}_{\hat{e}}$. It follows from (48) and (49) that

$$\begin{aligned}
\dot{V}_\upsilon &\le -\boldsymbol{e}^\top\boldsymbol{Q}_m\boldsymbol{e} + \frac{\hat{k}_s^*}{4}\nu + r\epsilon \\
&\le -2\mu_m V_\upsilon + 2\mu_m c + \frac{\hat{k}_s^*}{4}\nu + r\epsilon \\
&= -\mu_m V_\upsilon - \mu_m\big(V_\upsilon - 2\hat{c} - r\epsilon\big) \qquad (50)
\end{aligned}$$

where $\hat{c} = c + (\hat{k}_s^*\nu)/(8\mu_m)$. Recall that $t_{0,\upsilon}$ and $t_{f,\upsilon}$ denote the initial and the final time, respectively, of the υth mode. It follows from (48) that if $V_\upsilon(t) \ge 2\hat{c} + r\epsilon$ for $t \in [t_{0,\upsilon}, t_{f,\upsilon}] \cap [t_0 + T_1(\epsilon), t_0 + T_3)$, then $\dot{V}_\upsilon(t) \le -\mu_m V_\upsilon(t)$, which implies that for $t \in [t_{0,\upsilon}, t_{f,\upsilon}] \cap [t_0 + T_1(\epsilon), t_0 + T_3)$,

$$V_\upsilon(t) \le \exp(-\mu_m(t - t_{0,\upsilon}))V_\upsilon(t_{0,\upsilon}). \qquad (51)$$

Replacing $2\bar{c}$ with $2\hat{c} + r\epsilon$ in the proof of Theorem 1, the following corollary can be proved.

Corollary 3: Let t_1, t_2, and t_3 be three consecutive switching time instants in the interval $[t_0 + T_1(\epsilon), t_0 + T_3)$ so that $\upsilon = \upsilon_1$ for $t \in [t_1, t_2)$ and $\upsilon = \upsilon_2$ for $t \in [t_2, t_3)$. Suppose that $V_\upsilon(t)$ satisfies (51) and $V_\upsilon(t) \ge 2\hat{c} + r\epsilon$ for $t \in [t_1, t_3)$. If one of the following conditions are satisfied, then $V_{\upsilon_2}(t_2) < V_{\upsilon_1}(t_1)$ and $V_{\upsilon_2}(t_3^-) < V_{\upsilon_1}(t_2^-)$.

1) The dwell time T_d of the variable-structure RBF network is selected such that

$$T_d \ge \frac{1}{\mu_m}\ln\left(\frac{3}{2}\right). \qquad (52)$$

2) The constants c and ν satisfy the following inequality when T_d does not satisfy (52),

$$0 < c < \frac{\exp(\mu_m T_d) - 1}{3 - 2\exp(\mu_m T_d)}\left(\frac{k_s\nu}{4\mu_m} + r\epsilon\right). \qquad (53)$$

Theorem 3: For the system (2) driven by the proposed adaptive robust output feedback controller (42) with the adaptation laws (40), suppose that one of the conditions (52) or (53) is satisfied. If $c_e \geq c_{e_1} + c$ and $c_e > 2\hat{c} + c$, there exists a constant $\epsilon^* \in (0, 1)$ so that if $\epsilon \in (0, \epsilon^*)$, then $\boldsymbol{e}(t) \in \boldsymbol{\Omega}_e$ and $\boldsymbol{x}(t) \in \boldsymbol{\Omega}_x$ for $t \geq t_0$. Moreover, there exists a finite time $T \geq t_0 + T_1(\epsilon)$ such that

$$\frac{1}{2}\boldsymbol{e}(t)^\top \boldsymbol{P}_m \boldsymbol{e}(t) \leq 2\hat{c} + r\epsilon + c \tag{54}$$

with some $r > 0$ for $t \geq T$. In addition, suppose that there exists a finite time $T_s \geq t_0 + T_1(\epsilon)$ such that $v = v_s$ for $t \geq T_s$. Then, there exists a finite time $T \geq T_s$ such that

$$\frac{1}{2}\boldsymbol{e}^\top(t) \boldsymbol{P}_m \boldsymbol{e}(t) \leq 2\hat{c} + r\epsilon \tag{55}$$

for $t \geq T$.

Proof: Recall that if $\epsilon \in (0, \epsilon_2^*)$, then $\dot{V}_v(t)$ satisfies (50) for $t \in [t_0 + T_1(\epsilon), t_0 + T_3)$, where $V(t_0 + T_1(\epsilon)) \leq c_{e_1} + c$. If, at the same time, one of the conditions (52) or (53) is satisfied, then it follows from Corollary 3 that

$$\begin{aligned} V_v(t) &\leq \max\left\{V(t_0 + T_1(\epsilon)), 2\hat{c} + r\epsilon + c\right\} \\ &\leq \max\left\{c_{e_1} + c, 2\hat{c} + r\epsilon + c\right\} \end{aligned} \tag{56}$$

for $t \in [t_0 + T_1(\epsilon), t_0 + T_3)$. If $c_e > 2\hat{c} + c$, there exists a constant ϵ_3 so that if $\epsilon \in (0, \epsilon_3)$, then $c_e \geq 2\hat{c} + r\epsilon + c$. Let $\epsilon^* = \min\{\epsilon_2^*, \epsilon_3\}$. If $\epsilon \in (0, \epsilon^*)$ and $c_e \geq c_{e_1} + c$, then $V_v(t) \leq c_e$ for $t \in [t_0 + T_1(\epsilon), t_0 + T_3)$. Because $\frac{1}{2}\boldsymbol{e}(t)^\top \boldsymbol{P}_m \boldsymbol{e}(t) \leq V_v(t)$, it is true that $\frac{1}{2}\boldsymbol{e}(t)^\top \boldsymbol{P}_m \boldsymbol{e}(t) \leq c_e$, that is, $\boldsymbol{e} \in \boldsymbol{\Omega}_e$ for $t \in [t_0 + T_1(\epsilon), t_0 + T_3)$. Recall that $t_0 + T_3$ is the moment when the tracking error $\boldsymbol{e}(t)$ leaves the compact set $\boldsymbol{\Omega}_e$ for the first time. However, it follows from the above that $\boldsymbol{e}(t)$ will never leave the compact set $\boldsymbol{\Omega}_e$, which implies that $T_3 \to \infty$. Because $\boldsymbol{e}(t) \in \boldsymbol{\Omega}_e$ for $t \in [t_0, t_0 + T_1(\epsilon)]$, it is true that $\boldsymbol{e}(t) \in \boldsymbol{\Omega}_e$ and thus $\boldsymbol{x}(t) \in \boldsymbol{\Omega}_x$ for $t \geq t_0$. Let $T \geq t_0 + T_1(\epsilon)$ be the first time such that $V_v(T) \leq 2\hat{c} + r\epsilon$. Arguing in the same way as in the proof of Theorem 2, it can be obtained that $\frac{1}{2}\boldsymbol{e}(t)^\top \boldsymbol{P}_m \boldsymbol{e}(t) \leq 2\hat{c} + r\epsilon + c$ for $t \geq T$.

If, in addition, there exists a finite time $T_s \geq t_0 + T_1(\epsilon)$ such that $v = v_s$ for $t \geq T_s$, the arguments in Corollary 2 can be applied to show that there exists a finite time $T \geq T_s$ such that $\frac{1}{2}\boldsymbol{e}^\top(t) \boldsymbol{P}_m \boldsymbol{e}(t) \leq 2\hat{c} + r\epsilon$ for $t \geq T$. ■

It can be seen from (33), (34), (54), and (55) that the performance of the output feedback controller approaches that of the state feedback controller as ϵ approaches zero.

VI. Examples

In this section, the effectiveness of the proposed variable neural adaptive robust controllers is first demonstrated on the epoxy core linear motor described in [25] and the planar articulated two-link manipulator given in [26]. Then, the Duffing forced oscillation system as given in [6] is used to illustrate the performance of the proposed variable neural adaptive robust controllers on a time-varying system.

Example 1: In this example, the proposed state feedback controller is tested on the epoxy core linear motor described in [25]. The design model of this linear motor has the form

$$M\ddot{y} = u - B\dot{y} - A_f S_f(\dot{y}) + \eta.$$

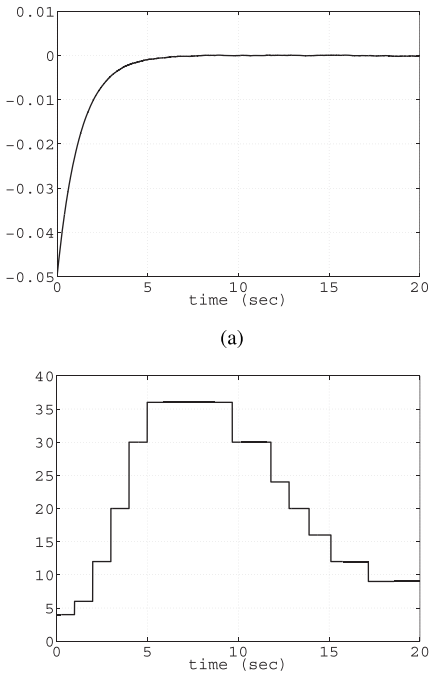

Fig. 3. State feedback controller performance in Example 1. (a) Output tracking error (m). (b) Variation of the number of grid nodes.

Here, M is the mass of the inertia load plus the coil assembly, y denotes the position of the inertia load, u denotes the input voltage to the motor, B is the equivalent viscous friction coefficient, $A_f S_f(\dot{y})$ is a continuous approximation of the discontinuous friction, and

$$\eta = B\dot{y} + A_f S_f(\dot{y}) - F(y, \dot{y}) + F_d$$

represents the lumped disturbance, where $F(y, \dot{y})$ is the lumped effect of friction and ripple forces and F_d represents the external disturbance such as cutting force in machine. The identified system parameters are $M = 0.1$ V/m/s^2, $B = 0.273$ V/m/s, and $A_f = 0.09$ V with

$$S_f(\dot{y}) = \frac{2}{\pi}\arctan(900\dot{y}).$$

Moreover, $0.02\ V/m/s^2 \leq M \leq 0.12$ V/m/s^2, $|u| \leq 2$ V, and $|\eta| \leq 2$ V. The linear motor is initially at rest, that is, $y = \dot{y} = 0$.

The reference signal is selected to be $y_d = 0.05\cos(4t)$. For this reference signal, the grid boundaries for y and $\dot{y}$ are chosen to be $[-0.1\ 0.1]$ and $[-0.4\ 0.4]$, respectively. The parameters of the controller are selected as $\boldsymbol{K} = [4\ 4]$, $\boldsymbol{Q}_m = 0.5\boldsymbol{I}_2$, $\underline{g} = 1/0.12$, $\boldsymbol{G}_0 = 20$, $d_f = 30$, $d_g = 30$, $d_o = 100$, and $\nu = 0.001$. The remaining design parameters of the variable-structure RCRBF network are selected as $e_{\max} = 0.0005$, $\rho = 0.2$, $\varrho = 0.1$, $\boldsymbol{d}_{\text{threshold}} = [0.01\ 0.01]$, $\underline{\omega}_1 = \underline{\omega}_2 = -10$, $\overline{\omega}_1 = \overline{\omega}_2 = 10$, $\kappa = 100$, and $T_d = 1.0$ so that $T_d > \ln(3/2)/\mu_m = 0.9252$, where $\mu_m = 0.4383$. It can be seen in Fig. 3(a) that the trajectory of the tracking error enters a neighborhood around the origin and stays there thereafter. The maximum output tracking error is bounded by 0.0005. Thus, the proposed variable neural adaptive robust state feedback

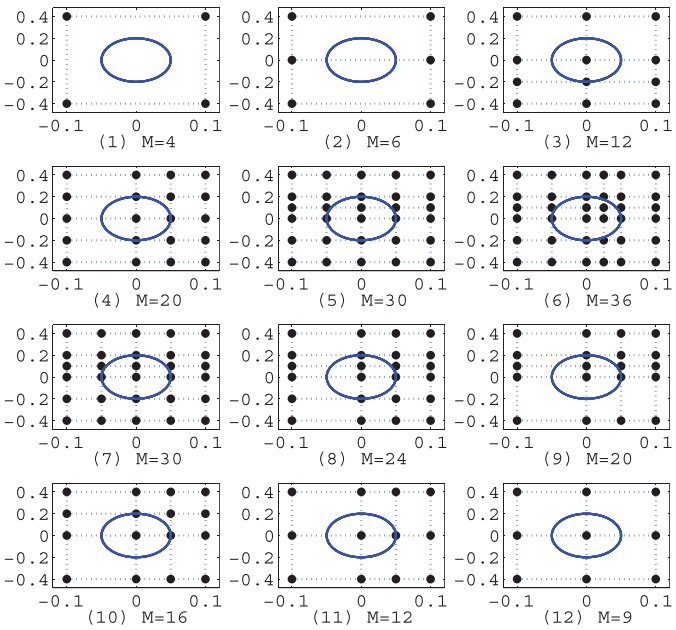

Fig. 4. Variation of the center grid in Example 1, where the ellipses are the phase portraits of the reference signal.

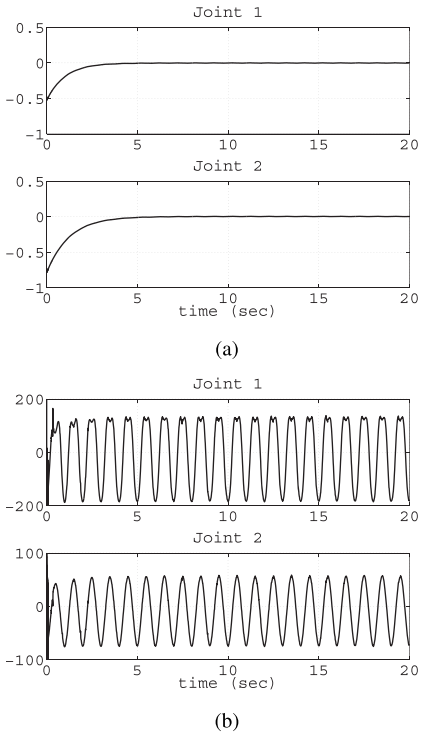

Fig. 5. Output feedback controller performance in Example 2. (a) Output tracking errors (rad). (b) Control inputs (N · m).

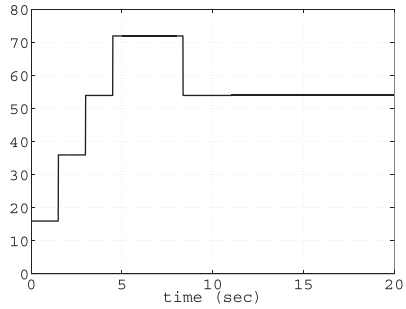

Fig. 6. Variation of the number of grid nodes in Example 2.

controller performs, as predicted by Theorem 2. The variation of the number of hidden neurons is shown in Fig. 3(b), while the variation of the center grid is shown in Fig. 4. When the tracking performance is poor, the network adds more RBFs to improve the approximation accuracy. When the tracking performance is acceptable, the network removes RBFs to avoid network redundancy.

Example 2: In this example, the proposed controller on a planar articulated two-link manipulator is tested. Let q_i and τ_i denote the angular position and the applied torque of the i-th joint, respectively, and let η_i denote the disturbance associated with τ_i. Then, the model of the two-link manipulator, which can be found in [33, p. 394], has the form

$$\begin{bmatrix} H_{11} & H_{12} \\ H_{21} & H_{22} \end{bmatrix} \begin{bmatrix} \ddot{q}_1 \\ \ddot{q}_2 \end{bmatrix} + \begin{bmatrix} -h\dot{q}_2 & -h\,(\dot{q}_1+\dot{q}_2) \\ h\dot{q}_1 & 0 \end{bmatrix} \begin{bmatrix} \dot{q}_1 \\ \dot{q}_2 \end{bmatrix} = \begin{bmatrix} \tau_1+\eta_1 \\ \tau_2+\eta_2 \end{bmatrix}$$

where $H_{11} = a_1 + 2a_3\cos(q_2) + 2a_4\sin(q_2)$, $H_{12} = H_{21} = a_2 + a_3\cos(q_2) + a_4\sin(q_2)$, $H_{22} = a_2$, $h = a_3\sin(q_2) - a_4\cos(q_2)$ with $a_1 = I_1 + m_1 l_{c1}^2 + I_e + m_e l_{ce}^2 + m_e l_1^2$, $a_2 = I_e + m_e l_{ce}^2$, $a_3 = m_e l_1 l_{ce}\cos(\delta_e)$, and $a_4 = m_e l_1 l_{ce}\sin(\delta_e)$. The same model was also used in [9], [12] but without input disturbances, that is, $\eta_1 = \eta_2 = 0$. The same numerical values as in [9], [12], and [33, p. 396] are used, that is, $m_1 = 1.0$ (kg), $m_e = 2.0$ (kg), $I_1 = 0.12$ (kg·m^2), $I_e = 0.25$ (kg·m^2), $l_{c1} = 0.5$ (m), $l_{ce} = 0.6$ (m), $l_1 = 1$ (m), and $\delta_e = \pi/6$ (rad). The input disturbances η_1 and η_2 are selected to be the band-limited white noise signals with noise power of 0.2 and 0.05, respectively, and sample time of 0.1. The manipulator is initially at rest, that is, $q_1 = q_2 = \dot{q}_1 = \dot{q}_2 = 0$.

It is assumed that only the system outputs are available. The reference signals were selected as $q_{d1}(t) = \frac{\pi}{6}\cos(2\pi t)$ and $q_{d2}(t) = \frac{\pi}{4}\cos(2\pi t)$. For the above reference signals, the grid boundaries for q_1, $\dot{q}_1$, q_2, and $\dot{q}_2$ are chosen to be $[-1.0\ 1.0]$, $[-4.0\ 4.0]$, $[-1.0\ 1.0]$, and $[-5.5\ 5.5]$, respectively. The parameters of the controller are selected to be $\boldsymbol{k}_1 = [1\ 2]$, $\boldsymbol{k}_2 = [4\ 4]$, $\boldsymbol{Q}_{m1} = \boldsymbol{Q}_{m2} = 0.5\boldsymbol{I}_2$, $\underline{g} = 0.1$, $\boldsymbol{G}_0 = 2\boldsymbol{I}_2$, $d_f = d_g = d_o = 5$, and $\nu = 0.025$. The remaining design parameters of the variable-structure RCRBF network were selected as $e_{\max} = 0.005$, $\rho = 0.8$, $\varrho = 0.3$, $\boldsymbol{d}_{\text{threshold}} = [0.1\ 0.4\ 0.1\ 0.55]$, $\underline{\omega}_1 = \underline{\omega}_2 = -25$, $\overline{\omega}_1 = \overline{\omega}_2 = 25$, $\kappa = 500$, and $T_d = 1.5$ so that $T_d > \ln(3/2)/\mu_m = 1.3843$, where $\mu_m = 3.4142$. The parameters for the high-gain observer are selected to be $\alpha_{11} = \alpha_{21} = 2$, $\alpha_{12} = \alpha_{22} = 1$, and $\epsilon = 10^{-4}$. In addition, $U_1 = 250$ and $U_2 = 150$. It can be seen from Figs. 5 and 6 that the output feedback controller performs as expected. The maximum output tracking errors are bounded by 0.005. Actually, the performance of the output feedback controller is similar to that of the state feedback controller, whose simulation results are not included due to space limitation.

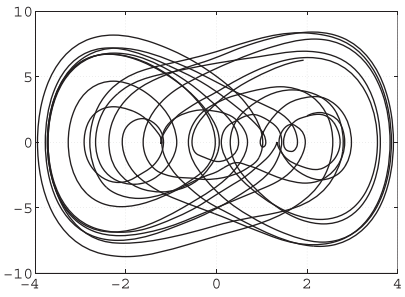

Fig. 7. Phase portrait of the uncontrolled system in Example 3.

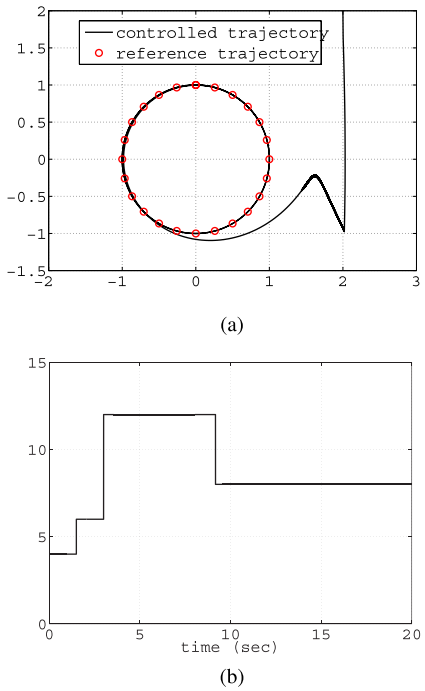

(a)

(b)

Fig. 8. Output feedback controller performance in Example 3. (a) Phase portrait of the controlled system. (b) Variation of the number of grid nodes.

Example 3: In this simulation, the performance of the proposed output feedback controller is further tested on the Duffing forced oscillation system [6], which has time-varying dynamics modeled by

$$\begin{cases} \dot{x}_1 = x_2 \\ \dot{x}_2 = -0.1x_2 - x_1^3 + 12\cos(t) + u + d. \end{cases}$$

The initial conditions are selected to be $x_1(0) = x_2(0) = 2$, and the disturbance d is chosen to be the colored noise signal, which is generated by passing the band-limited white noise signal with noise power of 0.2 through a low-pass filter. The phase portrait of the Duffing forced oscillation system with zero input for the time period $[0, 50]$ is shown in Fig. 7. The reference signal is selected to be $y_d(t) = \sin(t)$. The grid boundaries for y and $\dot{y}$ are chosen to be $[-2.5\ 2.5]$ and $[-2.5\ 2.5]$, respectively. The parameters for the controller are chosen to be $\boldsymbol{K} = [1\ 2]$, $\boldsymbol{Q}_m = 0.5\boldsymbol{I}_2$, $\underline{g} = 1$, $\boldsymbol{G}_0 = 1$, $d_f = 15$, $d_g = 2$, $d_o = 5$, and $\nu = 0.001$. The remaining design parameters of the variable-structure RCRBF network are selected as $e_{\max} = 0.0005$, $\rho = 0.2$, $\varrho = 0.1$, $\boldsymbol{d}_{\text{threshold}} = [0.2\ 0.2]$, $\underline{\omega}_1 = \underline{\omega}_2 = -10$, $\overline{\omega}_1 = \overline{\omega}_2 = 10$, $\kappa = 100$, and $T_d = 1.5$ so that $T_d > 1/\mu_m \ln(3/2) = 1.3843$, where $\mu_m = 0.2929$. The parameters for the high-gain observer are $\alpha_1 = 10$, $\alpha_2 = 25$, and $\epsilon = 10^{-3}$. It can be seen from Fig. 8 that the proposed variable neural adaptive robust control strategies are also effective for the output tracking of time-varying systems, such as the Duffing forced oscillation system. In this example, the maximum output tracking error is bounded by 0.002.

VII. Conclusion

Variable neural adaptive robust control strategies were proposed for the output tracking control for a class of MIMO uncertain systems. The variable-structure RBF network that can grow or shrink online dynamically according to the tracking performance was proposed for the self-organizing approximation of unknown system dynamics. The piecewise quadratic Lyapunov function was employed in the stability analysis of the closed-loop system to take into account the structure variation of the RBF network. The simulation results illustrate the effectiveness of the proposed variable neural adaptive robust controllers.

The MIMO system considered herein has been often referred to as the square system because the number of inputs and the number of outputs are the same. An open research problem is the design of adaptive robust controllers for the more general class of nonsquare MIMO uncertain systems. For these general systems, the proposed variable-structure RBF network for unknown function approximation can still be applied, and the proposed switched system approach for stability analysis will be modified accordingly.

References

[1] I. Kanellakopoulos, P. V. Kokotović, and R. Marino, "An extended direct scheme for robust adaptive nonlinear control," *Automatica*, vol. 27, no. 2, pp. 247–255, 1991.

[2] A. Kojić and A. M. Annaswamy, "Adaptive control of nonlinearly parameterized systems with a triangular structure," *Automatica*, vol. 38, no. 1, pp. 115–123, 2002.

[3] M. Krstić and P. V. Kokotović, "Adaptive nonlinear design with controller-identifier separation and swapping," *IEEE Trans. Autom. Control*, vol. 40, no. 3, pp. 426–460, Mar. 1995.

[4] E. B. Kosmatopoulos and P. A. Ioannou, "Robust switching adaptive control of multi-input nonlinear systems," *IEEE Trans. Autom. Control*, vol. 47, no. 4, pp. 610–624, Apr. 2002.

[5] R. M. Sanner and J.-J. E. Slotine, "Gaussian networks for direct adaptive control," *IEEE Trans. Neural Netw.*, vol. 3, no. 6, pp. 837–863, Nov. 1992.

[6] L.-X. Wang, "Stable adaptive fuzzy control of nonlinear systems," *IEEE Trans. Fuzzy Syst.*, vol. 1, no. 2, pp. 146–155, May 1993.

[7] A. Yeşildirek and F. L. Lewis, "Feedback linearization using neural networks," *Automatica*, vol. 31, no. 11, pp. 1659–1664, 1995.

[8] S. Seshagiri and H. K. Khalil, "Output feedback control of nonlinear systems using RBF neural networks," *IEEE Trans. Neural Netw.*, vol. 11, no. 1, pp. 69–79, Jan. 2000.

[9] C.-C. Liu and F.-C. Chen, "Adaptive control of non-linear continuous-time systems using neural networks—General relative degree and MIMO cases," *Int. J. Control*, vol. 58, no. 2, pp. 317–335, 1993.

[10] Y.-C. Chang, "An adaptive H^∞ tracking control for a class of nonlinear multiple-input multiple-output (MIMO) systems," *IEEE Trans. Autom. Control*, vol. 46, no. 9, pp. 1432–1437, Sep. 2001.

[11] S. Tong and H.-X. Li, "Fuzzy adaptive sliding-mode control for MIMO nonlinear systems," *IEEE Trans. Fuzzy Syst.*, vol. 11, no. 3, pp. 354–360, Jun. 2003.

[12] H. Xu and P. A. Ioannou, "Robust adaptive control for a class of MIMO nonlinear systems with guaranteed error bounds," *IEEE Trans. Autom. Control*, vol. 48, no. 5, pp. 728–742, May 2003.

[13] C. P. Bechlioulis and G. A. Rovithakis, "Robust adaptive control of feedback linearizable MIMO nonlinear systems with prescribed performance," *IEEE Trans. Autom. Control*, vol. 53, no. 9, pp. 2090–2099, Oct. 2008.
[14] H. K. Khalil, "Adaptive output feedback control of nonlinear systems represented by input-output models," *IEEE Trans. Autom. Control*, vol. 41, no. 2, pp. 177–188, Feb. 1996.
[15] S. Fabri and V. Kadirkamanathan, "Dynamic structure neural networks for stable adaptive control of nonlinear systems," *IEEE Trans. Neural Netw.*, vol. 7, no. 5, pp. 1151–1167, Sep. 1996.
[16] J.-H. Park, S.-H. Huh, S.-H. Kim, S.-J. Seo, and G.-T. Park, "Direct adaptive controller for nonaffine nonlinear systems using self-structuring neural networks," *IEEE Trans. Neural Netw.*, vol. 16, no. 2, pp. 414–422, Mar. 2005.
[17] Y. Zhao and J. A. Farrell, "Self-organizing approximation-based control for higher order systems," *IEEE Trans. Neural Netw.*, vol. 18, no. 4, pp. 1220–1231, Jul. 2007.
[18] J.-X. Xu and Y. Tan, "Nonlinear adaptive wavelet control using constructive wavelet networks," *IEEE Trans. Neural Netw.*, vol. 18, no. 1, pp. 115–127, Jan. 2007.
[19] J. Lian, Y. Lee, and S. H. Żak, "Variable neural direct adaptive robust control of uncertain systems," *IEEE Trans. Autom. Control*, vol. 53, no. 11, pp. 2658–2664, Dec. 2008.
[20] G. P. Liu, V. Kadirkamanathan, and S. A. Billings, "Variable neural networks for adaptive control of nonlinear systems," *IEEE Trans. Syst., Man, Cybern. C, Appl. Rev.*, vol. 29, no. 1, pp. 34–43, Feb. 1999.
[21] J. Lian, Y. Lee, S. D. Sudhoff, and S. H. Żak, "Self-organizing radial basis function network for real-time approximation of continuous-time dynamical systems," *IEEE Trans. Neural Netw.*, vol. 19, no. 3, pp. 460–474, Mar. 2008.
[22] J. P. Hespanha and A. S. Morse, "Stability of switched systems with average dwell-time," in *Proc. 38th Conf. Decision Control*, Phoenix, AZ, USA, Dec. 1999, pp. 2655–2660.
[23] M. S. Branicky, "Multiple Lyapunov functions and other analysis tools for switched and hybrid systems," *IEEE Trans. Autom. Control*, vol. 43, no. 4, pp. 475–482, Apr. 1998.
[24] M. Johansson and A. Rantzer, "Computation of piecewise quadratic Lyapunov functions for hybrid systems," *IEEE Trans. Autom. Control*, vol. 43, no. 4, pp. 555–559, Apr. 1998.
[25] L. Xu and B. Yao, "Adaptive robust precision motion control of linear motors with negligible electrical dynamics: Theory and experiments," *IEEE/ASME Trans. Mechatronics*, vol. 6, no. 4, pp. 444–452, Dec. 2001.
[26] J. J. Craig, *Introduction to Robotics: Mechanics and Control*. Reading, MA, USA: Addison-Wesley, 1986.
[27] R. J. Schilling, J. J. Carroll, and A. F. Al-Ajlouni, "Approximation of nonlinear systems with radial basis function neural networks," *IEEE Trans. Neural Netw.*, vol. 12, no. 1, pp. 1–15, Jan. 2001.
[28] B. Yao, "Integrated direct/indirect adaptive robust control of SISO nonlinear systems in semi-strict feedback form," in *Proc. Amer. Control Conf.*, vol. 4. Denver, CO, USA, Jun. 2003, pp. 3020–3025.
[29] M. M. Polycarpou and P. A. Ioannou, "On the existence and uniqueness of solutions in adaptive control systems," *IEEE Trans. Autom. Control*, vol. 38, no. 3, pp. 474–479, Mar. 1993.
[30] N. A. Mahmoud and H. K. Khalil, "Asymptotic regulation of minimum phase nonlinear systems using output feedback," *IEEE Trans. Autom. Control*, vol. 41, no. 10, pp. 1402–1412, Oct. 1996.
[31] H. K. Khalil, *Nonlinear Systems*, 2nd ed. Upper Saddle River, NJ, USA: Prentice-Hall, 1996.
[32] F. Esfandiari and H. K. Khalil, "Output feedback stabilization of fully linearizable systems," *Int. J. Control*, vol. 56, no. 5, pp. 1007–1037, 1992.
[33] J.-J. Slotine and W. Li, *Applied Nonlinear Control*. Englewood Cliffs, NJ, USA: Prentice-Hall, 1991.

Jianming Lian (S'08–M'10) received the B.S. degree in automation from the University of Science and Technology of China, Hefei, China, in 2004, and the M.S. and Ph.D. degrees in electrical engineering from Purdue University, West Lafayette, IN, USA, in 2007 and 2009, respectively.

He was a Post-Doctoral Research Associate with the Center for Advanced Power Systems, Florida State University, Tallahassee, FL, USA, from 2010 to 2011, where he was involved in various projects related to the development of future all-electric ship supported by Office of Naval Research. He is currently a Senior Engineer with the Electricity Infrastructure Group, Pacific Northwest National Laboratory, Richland, WA, USA. His current research interests include power system stability analysis and real-time control, load modeling and demand response, and nonlinear system analysis and control, in particular, adaptive control and decentralized control.

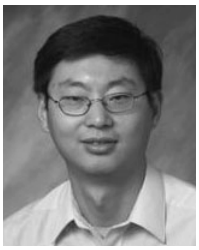

Jianghai Hu (S'99–M'04) received the B.E. degree in automatic control from Xi'an Jiaotong University, Xi'an, China, in 1994, and the M.A. degree in mathematics and the Ph.D. degree in electrical engineering from the University of California at Berkeley, Berkeley, CA, USA, in 2002 and 2003, respectively.

He joined the School of Electrical and Computer Engineering, Purdue University, West Lafayette, IN, USA, as an Assistant Professor in 2004, where he is currently an Associate Professor. His current research interests include hybrid systems, multiagent coordinated control, control of systems with uncertainty, and applied mathematics.

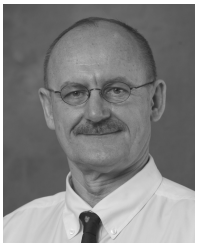

Stanislaw H. Żak (M'81) received the Ph.D. degree from the Warsaw University of Technology, Warsaw, Poland, in 1977.

He was an Assistant Professor with the Institute of Control and Industrial Electronics, Warsaw University of Technology, from 1977 to 1980. From 1980 to 1983, he was a Visiting Assistant Professor with the Department of Electrical Engineering, University of Minnesota, Minneapolis, MN, USA. In 1983, he joined the School of Electrical and Computer Engineering, Purdue University, West Lafayette, IN, USA, where he is currently a Professor. He has been involved in various areas of control, optimization, fuzzy systems, and neural networks. He has co-authored *Topics in the Analysis of Linear Dynamical Systems* (Warsaw, Poland: Polish Scientific Publishers, 1984) and *An Introduction to Optimization–4th Edition* (New York, NY, USA: Wiley, 2001) and has authored *Systems and Control* (London, U.K., Oxford University Press, 2003).

Prof. Żak was the Associate Editor of *Dynamics and Control* and the IEEE TRANSACTIONS ON NEURAL NETWORKS.